CHALMERS

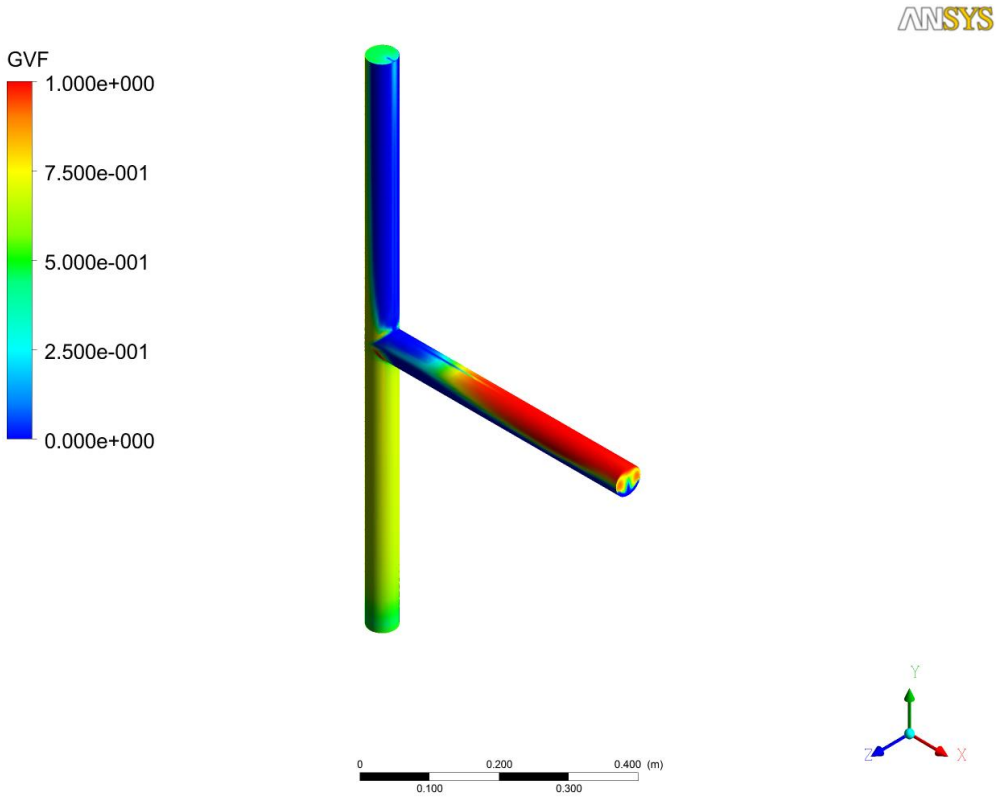

On Multiphase Flow Models in ANSYS CFD Software

Master's Thesis in Applied Mechanics

ELIN STENMARK

Department of Applied Mechanics
Division of Fluid Dynamics
CHALMERS UNIVERSITY OF TECHNOLOGY
Göteborg, Sweden 2013
Master's thesis 2013:11

MASTER'S THESIS IN APPLIED MECHANICS

On Multiphase Flow Models in ANSYS CFD Software

ELIN STENMARK

Department of Applied Mechanics
Division of Fluid Dynamics
CHALMERS UNIVERSITY OF TECHNOLOGY
Göteborg, Sweden 2013

On Multiphase Flow Models in ANSYS CFD Software
ELIN STENMARK

Master's Thesis 11
ISSN 1652-8557
Department of Applied Mechanics
Division of Fluid Dynamics
Chalmers University of Technology
SE-412 96 Göteborg
Sweden
Telephone: + 46 (0)31-772 1000

Cover:
Volume fraction of air in vertical T-junction with horizontal branch.

Chalmers Reproservice / Department of Applied Mechanics
Göteborg, Sweden 2013

On Multiphase Flow Models in ANSYS CFD Software
Master's Thesis in Applied Mechanics
ELIN STENMARK
Department of Applied Mechanics
Division of Fluid Dynamics
Chalmers University of Technology

ABSTRACT

Multiphase flow is a common phenomenon in many industrial processes, amongst them the oil and gas industry. Due to the complexity of multiphase flow, development of reliable analysis tool is difficult. Computational fluid dynamics (CFD) has been an established tool for flow analysis in the field of single phase flow for more than 20 years but has only started to become established in the multiphase field as well. To be able to use CFD in a meaningful way it is important to investigate, understand and validate the many models offered in commercial codes. The purpose of this thesis is to compare multiphase models available in the ANSYS software Fluent and CFX and perform simulations using the different models. The simulations were based on an experimental study concerning air-water mixtures in a vertical T-junction with horizontal branch. When a gas-liquid mixture flows into a branching pipe junction phase redistribution will occur and a higher proportion of gas will enter the side branch. The aim of the simulations was to find models/settings that accurately predict the phase redistribution phenomenon and investigate the effect of changing simulation parameters. This was done by systematically changing parameters and validating the results against the experimental data. Based on the simulations, it was evident that the Euler-Euler modelling approach was best suited for predicting the phase redistribution phenomenon in the T-junction. The choice of dispersed phase diameter was found to have the largest effect on the results. Generally, the predicted average volume fraction in each arm was in quite good consistency with experimental data while the predicted velocities were in low agreement. However, adding models to account for polydispersed flow increased the agreement also for the velocity.

Key words: Multiphase, Computational fluid dynamics, T-junction, Phase redistribution, Euler-Euler, VOF

Contents

Preface

In this thesis, the use of multiphase flow models in ANSYS CFD software has been investigated. The work has been carried out from January 2013 to June 2013 at Aker Solutions in Gothenburg in collaboration with the Division of Fluid Dynamics at the Department of Applied Mechanics, Chalmers, Sweden.

I am very grateful to Aker Solutions for giving me the possibility to do this work. Many thanks go out to my supervisor at Aker Solutions, Ph.D. Jonas Bredberg, for all the support and the many ideas. Thanks to everybody at Aker Solutions, especially the EST group, for making me feel welcome. I would like to express my greatest appreciation to Professor Lars Davidson at the Division of Fluid Dynamics for being willing to take on the role as examiner for this thesis and for helping me with finding this interesting project. Great thanks also go out to Docent Srdjan Sasic at the division of Fluid Dynamics for helpful ideas and comments.

Last but not least, thank you Sami Säkkinen for always supporting me and for being my best friend.

Notations

Greek symbols

α	Volume fraction
ρ	Density
$\boldsymbol{\tau}$	Viscous stress tensor

Roman symbols

B_B	Birth due to breakage
B_C	Birth due to coalescence
D_B	Death due to breakage
D_C	Death due to coalescence
G	Growth term
$\mathbf{g}$	Gravity
n	Number density of particles
$\mathbf{p}$	Instantaneous pressure
$\mathbf{P}$	Mean pressure shared between the phases
$\mathbf{S}$	Source term
$\mathbf{u}$	Instantaneous velocity
$\mathbf{U}$	Mean velocity
V	Volume
y^+	Dimensionless distance from the wall

Abbreviations

CFD	Computational Fluid Dynamics
DNS	Direct Numerical Simulations
FMV	Finite Volume Method
GVF	Gas Volume Fraction
HRIC	High Resolution Interface Capturing
IAC	Interfacial Area Concentration
MUSIG	Multiple Size Group
PBM	Population Balance Model
QMOM	Quadrature Method of Moments

SIMPLE	Semi-Implicit Method for Pressure-Linked Equations
SST	Shear Stress Transport
SSM	Standard Method of Moments
VOF	Volume of Fluid

Subscripts

B	Breakage
C	Coalescence
f	Fluid phase
k	k:th phase
m	Mixed properties
mass	Mass
p	Particle phase

1 Introduction

Multiphase flow is common in many industrial processes, amongst them the oil and gas industry. Enormous quantities of oil and gas are consumed on a daily basis (CIA 2013) and even a slight enhancement in extraction efficiency will have a significant influence on revenues for companies in the oil and gas industry. Hence, finding reliable analysis tools for understanding and optimisation of multiphase flows is a priority for these companies. One of these companies is Aker Solutions, where computational fluid dynamics (CFD) is used in the development of subsea equipment.

CFD was developed during the second half of the 20^{th} century and became an established analysis tool for single-phase flow calculations during the 90ies with the appearance of commercial CFD software such as ANSYS Fluent and ANSYS CFX. The use of CFD in the area of multiphase flow is not as established. However, with the development of computer resources, making more complex analyses possible, along with the incorporation of multiphase flow models in commercial codes such as those previously mentioned, CFD is now gaining more importance also in this field (Crowe et. al 2012).

Several error sources exist for numerical simulations. Numerical approximation errors will always occur but another error source, which often is difficult to detect, is usage error. Unintended application of models, badly chosen parameters or wrongfully applied boundary conditions can lead to unphysical and inaccurate results. With the extended use of CFD simulations in engineering work it is of high importance to investigate the accuracy of commercial codes as well as understanding the choice of models. This is particularly important for multiphase flow where the complexity of both physical laws and numerical treatment makes the development of general models difficult (Wachem and Almstedt 2003).

Not much published work has been done on comparing commercial CFD codes and as models and codes may be intended and developed for a certain multiphase area, what is accurate and applicable for one business area might be unsuitable to use for another area. Therefore, there is a need to examine and compare the models available to create a knowledge base for multiphase flow simulations using commercial software in the oil and gas industry.

1.1 Objective

The objective of this thesis is to, through numerical simulations and validation against experimental data, build up a knowledge base that can be used for defining multiphase CFD procedures at Aker Solutions. Multiphase models available in ANSYS CFD software will be investigated to find their usefulness for different flow cases as well as their limitations. Simulations will be performed with systematic parameterisation to investigate the effect of changing models and parameters. The simulations will be based on an experimental study to enable validation of the results. The findings of the model survey and simulations will result in general recommendations for multiphase CFD simulations including guidance on the effect of choice of models, settings etcetera.

1.2 Delimitations

Only the multiphase models available in the ANSYS CFD codes CFX and Fluent will be investigated. The reason for this delimitation is that this is the software presently used for flow simulations at Aker Solutions. Restrictions are also made in the number of models and settings that can be tested as it is not feasible to investigate all the models that are available in the ANSYS CFD software during the 20 weeks in which this project is to be carried out.

1.3 Thesis outline

This thesis is organised in eight chapters. After the introduction, Chapter 2 contains basic theory about fluid flow in general, multiphase flow and the most common modelling approaches for multiphase flow. In addition, some basic theory about CFD is given.

Chapter 3 presents the software used and in Chapter 4 a short review of the experiment used as benchmark for the simulations is given.

In Chapter 5 the methodology is described. Geometry, mesh, simulation settings and boundary conditions are presented and convergence and evaluation criteria are discussed.

The results are presented and discussed in Chapter 6 and in Chapter 7 conclusions from the study are drawn. Finally, the references are stated in Chapter 8.

2 Theory

Equations are used to mathematically describe the physics of fluid flow. The continuity equation and the momentum equation, also known as the Navier-Stokes equation, are needed to describe the state of any type of flow and are generally solved for all flows in CFD modelling, see equation 2.1 and 2.2, respectively (ANSYS CFX Solver Theory Guide 2011). Additional equations, such as for example the energy equation and/or turbulence equations, might be needed to properly describe a flow depending on the nature of the particular flow.

$$\frac{\partial \rho}{\partial t} + \nabla \cdot (\rho \mathbf{u}) = 0 \tag{2.1}$$

$$\frac{\partial \rho \mathbf{u}}{\partial t} + \nabla \cdot (\rho \mathbf{u}\mathbf{u}) = -\nabla p + \nabla \cdot \boldsymbol{\tau} + \rho \mathbf{g} \tag{2.2}$$

Here $\boldsymbol{\rho}$ is density, $\mathbf{u}$ is instantaneous velocity, $\mathbf{p}$ is pressure, $\boldsymbol{\tau}$ is the viscous stress tensor and $\mathbf{g}$ is the gravity vector.

Solving the governing equations without any modelling is called direct numerical simulations (DNS). Running DNS-simulations is very time consuming. In practice, all flows are turbulent and turbulent flow exhibits time scales of such significantly different magnitudes that the mesh resolution needs to be so fine that the calculation times become unfeasible. Therefore, modelling is often employed to account for the turbulent effects and the topic of turbulence modelling has been the main focus of single-phase CFD research for the last couple of years (Crowe et. al 2012).

Multiphase flow requires even further modelling due to the complex behaviour of interaction between the phases. Even when doing DNS-simulations for multiphase flow, modelling is needed. Section 2.1 gives the basics of multiphase flow and in Section 2.2 some of the fundamental concepts of CFD are given.

2.1 Multiphase flow theory

Multiphase flow is flow with simultaneous presence of different phases, where phase refers to solid, liquid or vapour state of matter. There are four main categories of multiphase flows; gas-liquid, gas-solid, liquid-solid and three-phase flows. Further characterisation is commonly done according to the visual appearance of the flow as

separated, mixed or dispersed flow. These are called flow patterns or flow regimes and the categorisation of a multiphase flow in a certain flow regime is comparable to the importance of knowing if a flow is laminar or turbulent in single-phase flow analysis (Thome 2004).

A flow pattern describes the geometrical distribution of the phases and the flow pattern greatly affects phase distribution, velocity distribution and etcetera for a certain flow situation. A number of flow regimes exist and the possible flow patterns differ depending on the geometry of the flow domain. For some simple shapes, for example horizontal and vertical pipes, the flow patterns that occur for different phase velocities etcetera have been summarised in a so called flow map. Figure 2.1 visualises the flow configuration for some possible flow regimes and Figure 2.2 shows an example of a flow maps for horizontal pipe flow.

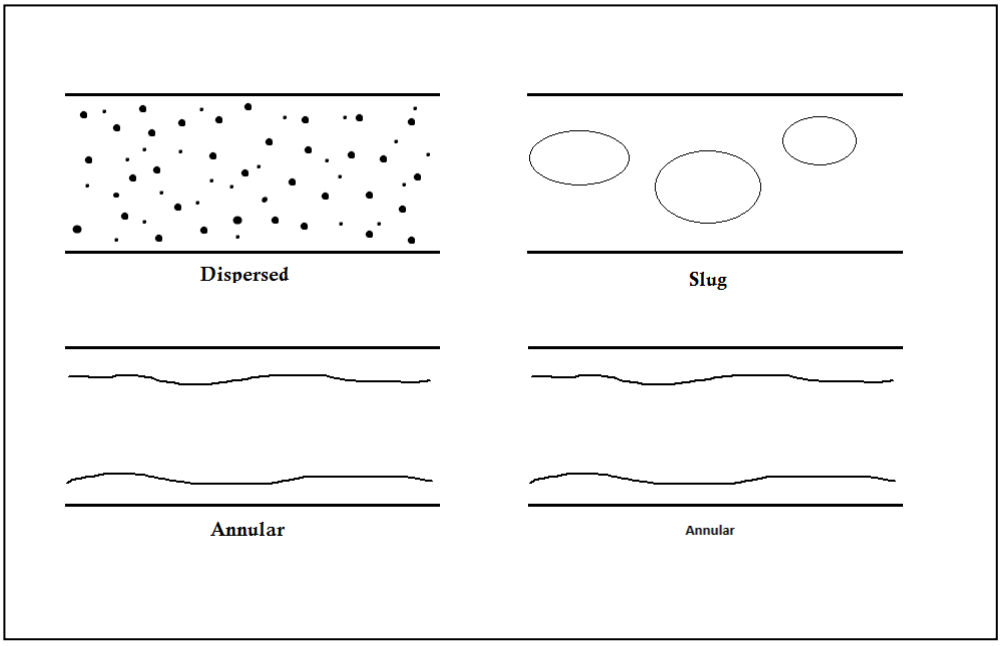

Figure 2.1 Example of typical flow patterns for flow in horizontal pipes

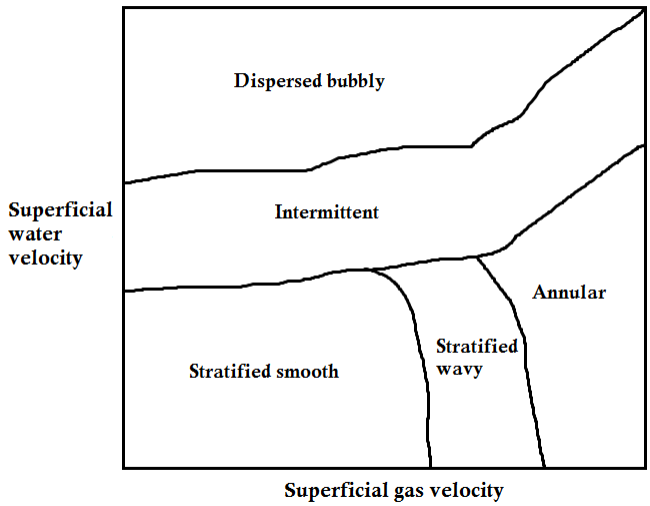

Figure 2.2 Example of flow map for two phase flow in horizontal pipes. Based on figure by Brill and Arlrachakaran (1992).

The two extremes on a flow map is dispersed flow and separated flow. In separated flow there is a distinct boundary between the phases. Examples of separated flow is stratified flow where one phase is flowing on top of another or annular flow in a pipe with a liquid film along the pipe and a gas core in the middle. Dispersed flow is flow where one phase is widely distributed as solid particles or bubbles in another continuous phase. Several intermediate regimes also exist, which contain both separated and dispersed phases such as for example annular bubbly flow. Due to growing instabilities in one regime, transition to another regime can occur. This phenomenon complicates the modelling of multiphase flow even further as the transition is unpredictable and the different flow regimes are to some extent governed by different physics.

2.1.1 Modelling approaches

Models are used to be able to describe and predict the physics of multiphase flow. As previously mentioned, modelling of multiphase flow is very complex. In addition, there are also limitations in time, computer capacity etcetera when performing numerical studies. This has led to the development of models that can account for different levels of information, meaning different levels of accuracy, and are suitable

for different multiphase flow applications. Some of these modelling approaches are presented below.

2.1.1.1 Euler-Lagrange approach

In the Euler-Lagrange approach, particles are tracked on the level of a single particle where particle refers to either a solid particle or a gas/fluid bubble/droplet. Conservation equations are solved for the continuous phase and the particle phase is tracked by solving the equations of motion for each particle, see equations 2.3, 2.4 and 2.5 below.

$$\frac{\partial \alpha_f \rho_f}{\partial t} + \nabla \cdot (\alpha_f \rho_f \mathbf{u}_f) = \mathbf{S}_{mass} \tag{2.3}$$

$$\frac{\partial \alpha_f \rho_f}{\partial t} + \nabla \cdot (\alpha_f \rho_f \mathbf{u}_f \mathbf{u}_f) = \alpha_f \nabla \mathbf{p} - \alpha_f \nabla \cdot \boldsymbol{\tau}_f - \mathbf{S}_p + \alpha_f \rho_f \mathbf{g} = 0 \tag{2.4}$$

$$\frac{\partial \mathbf{u}_p}{\partial \mathrm{t}} = \sum \mathbf{F} \tag{2.5}$$

Here α is volume fraction, $\mathbf{S}_{mass}$ is a mass source term existing in the case of exchange of mass between the phases, $\mathbf{S}_p$ momentum source term existing in case of exchange of momentum between the phases and $\mathbf{F}$ is force. Subscript f and p refers to the fluid and particle phases, respectively.

The forces acting on particles vary depending on the flow situation. The drag force is generally included and other forces that can be of importance are for example lift force, virtual mass force and/or history force. When performing numerical modelling it is up to the modeller to judge which forces that are of importance to include on the right hand side of equation 2.5. Adding more forces to a model increases accuracy but also increases complexity. Coupling between the continuous phase and the dispersed phase is achieved through the source terms. These are included also in the equation for the dispersed phase but are not explicitly shown here as they are a part of the right hand side. Integration of equation 2.5 gives the location of the dispersed phase.

As this modelling approach resolves information on the level of a single particle it is quite computationally expensive. To decrease the computational cost one can choose to track clusters of particles instead. However, this approach is still computationally

expensive and therefore Euler-Lagrange modelling is suitable for dilute dispersed flow, meaning flows with a low volume fraction of the dispersed phase.

2.1.1.2 Euler-Euler approach

In Euler-Euler models all phases are treated as continuous. For that reason, these models are often also called multi-fluid models. Multi-fluid models are appropriate for separated flows where both phases can be described as a continuum. However, the Euler-Euler approach can also be used to model dispersed flows when the overall motion of particles is of interest rather than tracking individual particles. The dispersed phase equations are averaged in each computational cell to achieve mean fields. To be able to describe a dispersed phase as a continuum, the volume fraction should be high and hence this approach is suitable for dense flows.

The phases are treated separately and one set of conservation equations are solved for each phase. Coupling between the phases is achieved through a shared pressure and interphase exchange coefficients. The interphase exchange coefficients need to be modelled. Just as in the Euler-Lagrange approach it is up to the modeller to decide which interphase phenomena to include. A number of models, suitable for different flow types, have been developed in the literature. No details of interphase exchange modelling will be given here. In addition to the regular transport equations, a transport equation for the volume fraction is also solved for each phase. The sum of the volume fractions should be equal to one. The governing equations for a two-fluid model with two continuous phases are shown below.

$$\frac{\partial \alpha_k \rho_k}{\partial t} + \nabla \cdot (\alpha_k \rho_k \mathbf{U}_k) = 0 \tag{2.6}$$

$$\frac{\partial \alpha_k \rho_k \mathbf{U}_k}{\partial t} + \nabla \cdot (\alpha_k \rho_k \mathbf{U}_k \mathbf{U}_k) = -\alpha_k \nabla \mathbf{P} + \alpha_k \nabla \cdot \boldsymbol{\tau}_k + \alpha_k \rho_k \mathbf{g}_k + \mathbf{S}_k = 0 \tag{2.7}$$

$$\frac{\partial \alpha_k}{\partial t} + \nabla \cdot (\alpha_k \mathbf{U}_k) = 0 \tag{2.8}$$

Here $\mathbf{U}$ is the mean velocity field and $\mathbf{P}$ is the mean pressure shared by the phases. The subscript k refers to the k:th continuous phase.

A mixture model is a simplified version of an Euler-Euler model. As in the Euler-Euler models both phases are treated as interpenetrating continua but in the mixture model the transport equations are based on mixture properties, such as mixture velocity, mixture viscosity etcetera. To track the different phases, a transport equation for the volume fraction is also solved. The phases are allowed to move with different velocities by using the concept of slip velocity, which in turn includes further modelling.

2.1.1.3 Volume of fluid approach

A third modelling approach is the volume of fluid (VOF) method. VOF belongs to the Euler-Euler framework where all phases are treated as continuous, but in contrary to the previous presented models the VOF model does not allow the phases to be interpenetrating. The VOF method uses a phase indicator function, sometimes also called a colour function, to track the interface between two or more phases. The indicator function has value one or zero when a control volume is entirely filled with one of the phases and a value between one and zero if an interface is present in the control volume. Hence, the phase indicator function has the properties of volume fraction.

The transport equations are solved for mixture properties without slip velocity, meaning that all field variables are assumed to be shared between the phases. To track the interface, an advection equation for the indicator function is solved. In order to obtain a sharp interface the discretisation of the indicator function equation is crucial. Different techniques have been proposed for this. The equations solved in the VOF method are shown below.

$$\frac{\partial \rho_m}{\partial t} + \nabla \cdot (\rho_m \mathbf{u}) = 0 \tag{2.9}$$

$$\frac{\partial \rho_m \mathbf{u}}{\partial t} + \nabla(\rho_m \mathbf{u}\mathbf{u}) = -\nabla P + \nabla \boldsymbol{\tau} + \rho_m \mathbf{g} + \mathbf{S} = 0 \tag{2.10}$$

$$\frac{\partial \alpha}{\partial t} + \nabla(\alpha \mathbf{u}) = 0 \tag{2.11}$$

Here $\rho_m = \sum \alpha_k \rho_k$. The subscript m refers to mixture properties.

As the focus of the VOF method is to track the interface between two or more phases it is suitable for flows with sharp interfaces, such as slug, stratified or free-surface flows.

2.1.1.4 Dispersed phase modelling

In both the Eulerian-Lagrangian and the Eulerian-Eulerian approach, modelling is needed to describe the dispersed phase. The simplest and probably most common assumption, especially for two-fluid models, is to describe the dispersed phase as spherical particles that maintain a constant diameter throughout the entire flow regime. However, many practical problems concern polydispersed flow, meaning flow with particles of both varying shape and size. In addition, the particles can often change shape/size due to coalescence, breakup etcetera. This is common in for example bubbly flows.

Population balance models (PBMs) are rather advanced models that can be used to predict phenomena such as for example coalescence, nucleation and breakage of bubbles/droplets and size distribution of particles in a flow regime. In a PBM, population balance equations (PBEs) are solved to describe changes in the dispersed phase, in addition to the usual mass, momentum and energy equations, see equation 2.12.

$$\frac{\partial n(V,t)}{\partial t} + \nabla \cdot (\mathbf{u} n(V,t)) = B_B - D_B + B_C - D_C + G \qquad (2.12)$$

Here n represents the number density of particles of volume V at time t, B_B is birth due to breakage, D_B is death due to breakage, B_C is birth due to coalescence, D_C is death due to coalescence and G is a growth term.

Various techniques have been developed for solving equation 2.12 numerically and several models have also been developed to describe the terms on the right hand side. The ability to include the growth, breakage and coalescence terms and the way they are modelled might vary depending on the PBM solver technique. Implementing a PBM is computationally expensive due to the many transport equations solved and simplified, less computationally demanding, models have been proposed.

2.2 Computational fluid dynamics

The governing flow equations, presented in Section 2.1, are coupled non-linear partial differential equations. These can be solved analytically only for very simple cases. For real life flows one must use numerical methods to transform the equations into algebraic approximations. In computational fluid dynamics numerical approximations of the solutions to the governing equations are obtained using computers.

2.2.1 The finite volume method

A method for discretising the transport equations commonly implemented in CFD codes is the finite volume method (FVM). In a FVM, the computational domain is divided in control volumes and conservation principles are applied to each control volume. This ensures conservation, both in each cell and globally in the domain, which is a great advantage of the FVM. Using FVM also allows for the use of unstructured grids which decreases the computational time. Two versions of the FVM are presented in Sections 2.1.1.1 and 2.1.1.2 below.

2.2.1.1 Centre node based FVM

In a centre node based FVM, the computational domain is divided into a mesh where each element in the mesh makes up a control volume. The transport equations are integrated over each control volume and then discretised to obtain one set of algebraic equations for each control volume/cell. In the centre node based FVM approach, the value of each variable is stored in a node in the centre of the cell. However, the discretised equations also include values for the cell faces. Therefore, interpolation methods are used to obtain approximate values at these positions. The choice of interpolation method has a great impact on numerical stability, convergence rate and accuracy.

2.2.1.2 Vertex based FVM

In a vertex based FVM, control volumes are constructed around each mesh vertex, meaning each cell corner. The mesh vertices are also used to store the variables. Just as in the centre node based approach, the governing equations are integrated over each control volume. However, since a control volume lies within several mesh elements, discretisation is done within each element and then the properties are distributed to the corresponding control volume. To solve the discretised equations properties are needed for other locations than the mesh vertices. Approximations are needed and in the vertex based approach the concept of finite element shape functions is used to obtain these approximations. The appearance of the shape functions depend on the element type.

2.2.2 Coupled and segregated solvers

In the discretised form of the governing equations the pressure and velocity is strongly coupled. Pressure gradients appear in the momentum equations and hence the pressure distribution is needed to solve these equations. However, obtaining the pressure field is not completely straight forward. The momentum equations can be used to solve for the velocities if the pressure is known but the fourth equation, the continuity equation, cannot be used directly to obtain the pressure field. The fact that the pressure and velocity fields are coupled is an issue that needs to be dealt with in CFD codes. Two

main types of solvers exist for handling the pressure velocity coupling; segregated solvers and coupled solvers.

A segregated solver makes use of a pressure correction equation. Firstly, the momentum equations are solved using a guessed pressure. If the resulting velocities do not satisfy the continuity equation a pressure correction equation is solved to update the pressure field. With the updated pressure the velocity fields are also updated and this process is repeated until the obtained velocity fields satisfy both the momentum equations and the continuity equation. One of the most widely used pressure correction schemes is the SIMPLE (Semi Implicit Method for Pressure Linked Equations) scheme but a number of version exist. Due to the fact that the equations are solved in a subsequent manner only one discrete equation needs to be stored at a time which results in lower memory requirements. However, due to the iterative nature of the solution algorithm the convergence rate is often slower (ANSYS Fluent Theory Guide 2011).

In a coupled solver, the momentum and continuity equations are solved simultaneously. As the discrete system of all equations needs to be stored at the same time the memory requirement is larger for a coupled solver and it takes more time to complete one iteration loop. However, in return for taking more time for each iteration the total number of iterations to achieve convergence is usually lowered when using a coupled solver (ANSYS Fluent Theory Guide 2011).

3 Software

Two commercial CFD programmes were used and compared in this thesis, Fluent and CFX, both from ANSYS Inc. For geometry and mesh generation the ANSYS software ICEM CFD was used. In this section, a short description of the software is given.

3.1 ICEM CFD

ICEM CFD is a meshing software. It allows for the use of CAD geometries or to build the geometry using a number of geometry tools. In ICEM CFD a block-structured meshing approach is employed, allowing for hexahedral meshes also in rather complex geometries. Both structured and unstructured meshes can be created using ICEM CFD.

3.2 Fluent

The Fluent solver is based on the centre node FVM discretisation technique and offers both segregated and coupled solution methods. Three Euler-Euler multiphase models are available; the Eulerian model, the mixture model and the VOF model. In addition, one particle tracking model is available.

As mentioned in Section 2.1.1.3, the discretisation of the volume fraction equation is crucial in a VOF method to keep the interface sharp. The choice of discretisation method can have a great influence on the results in other multiphase models as well. To resolve this issue, Fluent has a number of discretisation techniques implemented specifically for the volume fraction equation. Several methods are also available for spatial discretisation of the other transport equations. To model interphase transfer there is both a number of drag models available along with other transfer mechanisms such as lift forces, turbulent dispersion etcetera.

Fluent offers three main approaches to model dispersed phases with a two-fluid formulation. With the default settings it is assumed that the dispersed phase has a constant diameter or a diameter defined by a user-defined function. With this setting, phenomena such as coalescence and breakage are not considered. To account for such

effects, either the add-on module Population Balance Model or the Interfacial Area Concentration (IAC) setting can be used. The PBM add-on module includes a number of methods for solving the PBE described in Section 2.1.1.4; the Discrete, the SMM (Standard Method of Moments) and the QMOM (Quadrature Method of Moments). In the discrete method, the size distribution is divided in to a number of size intervals. This method is useful when the range of particles sizes are known in advance but if a large number of intervals is needed it is quite computationally expensive. In the SMM, transport equations are solved for moments of the distribution, making it more computationally efficient as fewer equations are solved. The QMOM is based on the same approach as the SMM but includes modelling for certain terms that are directly solved in the SMM. This makes the QMOM applicable to a broader range of flow cases than the SMM (ANSYS Fluent Population Balance Module Manual 2011). A more detailed description of the polydispersed models offered in Fluent can be found in the ANSYS Fluent PBM manual (2011). Several options for modelling the growth, breakage and coalescence terms in the PBE are also available in the PBM module.

The IAC model is a simplified version of a PBM in which only one additional transport equation, an IAC transport equation, is solved per secondary phase. IAC is defined as the interfacial area between two phases per unit mixture volume. Phenomenon such as coalescence, breakage and nucleation can be modelled with the IAC model but the distribution of particle sizes cannot be predicted.

3.3 CFX

In CFX, only the coupled solver is implemented and the vertex based FVM approach is used for discretisation. Two main multiphase model are available; a homogeneous and an inhomogeneous model. The homogeneous corresponds to a VOF model. The inhomogeneous model is based on the Euler-Euler approach and can be used together with several subsidiary models to model dispersed flow, mixtures of continuous fluids etcetera.

In CFX, the same discretisation methods are available for all transport equations, including the volume fraction equation. A first order scheme, a blending scheme and a higher resolution scheme are available. Depending on the types of phases, for

example continuous or dispersed fluid, different interphase transfer models are made available.

To model polydispersed flows CFX offers a model called MUSIG (Multiple Size Group). The MUSIG model is based on solving the PBE described in Section 2.1.1.4. Only one method for solving the PBE is available and this is based on discretising the population distribution into a number of predefined size intervals. However, a number of methods for defining the size intervals are available, for example geometric, equal mass and equal diameter size distribution. A more detailed description of the MUSIG model can be found in the ANSYS CFX manual (2011).

4 Experimental study

The experimental study "Two phase flow through branching pipe junctions" by Davis and Fungtamasan (1990) was used as a benchmark for the CFD simulations to enable validation of the simulation results. The experiment concerns distribution of volume fraction, velocity and bubble size for a bubbly air-water mixture in a vertical T-junction with horizontal branch. A nearly uniform mixture with an average bubble diameter of 2mm entered a T-junction from beneath and was divided in two outlets. T-junctions are commonly encountered in pipeline systems, for example in oil fields, and when a multiphase flow enters a T-junction a redistribution of the phases often occurs. This redistribution can be desirable if a phase separation is required but for other situations the uneven phase distribution can lead to lowered extraction efficiency and other undesirable phenomena.

Using probes, Davis and Fungtamasan measured average velocity and volume fraction as well as local distribution of the same at cross sections 500 mm from the junction in each arm of the T-junction. A series of flow conditions with different inlet void fractions and/or mixture velocities was tested to investigate the effect of inlet conditions on phase distribution. The experiment showed that a higher proportion of gas generally tended to flow into the branch arm. This phenomenon has been identified also in several experiments concerning T-junctions (Mudde et al. 1993, Walters et al. 1998). Air is drawn into the branch arm and a recirculation zone with a high concentration of gas occurs directly after the junction in the lower part of the branch. Due to gravity effects, the phases separate further away from the junction and the lighter gas phase flows on top of the heavier water phase.

Davis and Fungtamasan found that the amount of gas that flowed into the branch arm increased with higher inlet volume fraction and higher inlet mixture velocity. Several experiments have also shown that the amount of gas drawn into the side arm is highly affected by the inlet flow pattern and the bulk flow split (Elazhary 2012, Mudde, et al. 1993, Walters et al. 1998). For comparison with CFD results, one set of inlet conditions from the article by Fungtamasan and Davis was chosen. These are presented in Section 5.2.

5 Method

In this section the methodology is presented. Firstly, the geometry and mesh are discussed. This is followed by the choice of simulations settings and a description of the boundary conditions. Lastly, the convergence and evaluation criteria are presented.

5.1 Geometry and Mesh

The domain and the meshes were created using ANSYS ICEM CFD. Three domains were created with dimensions taken from the experimental setup. For all three domains the inner diameter of the pipes was 50mm. In the first domain, all three pipe arms were made 500mm long. A second domain with a prolonged branch arm, length 1000mm, was also created since reversed flow occurred at the branch outlet for some cases. The prolonged domain was used to avoid the reversed flow for these cases. A third domain was needed for simulations with homogeneous/VOF models. As it is assumed that one velocity field is shared between the phases in these models separate inlets were needed for the phases to be able to set different inlet velocities. The air was injected into the water through several evenly distributed holes. To allow the phases to mix and develop before entering the junction the inlet was located 1800mm below the junction in accordance with the location of the mixer in the experiment. The computational domains are presented in Figures 5.1, 5.2 and 5.3.

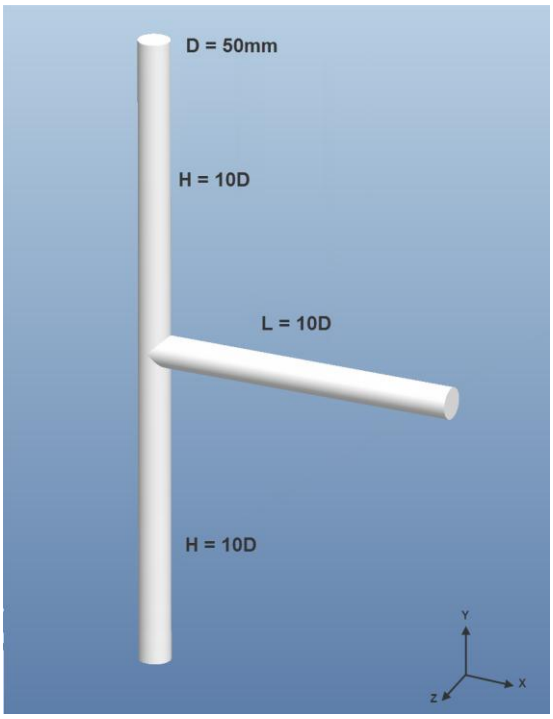

Figure 5.1 Original computational domain

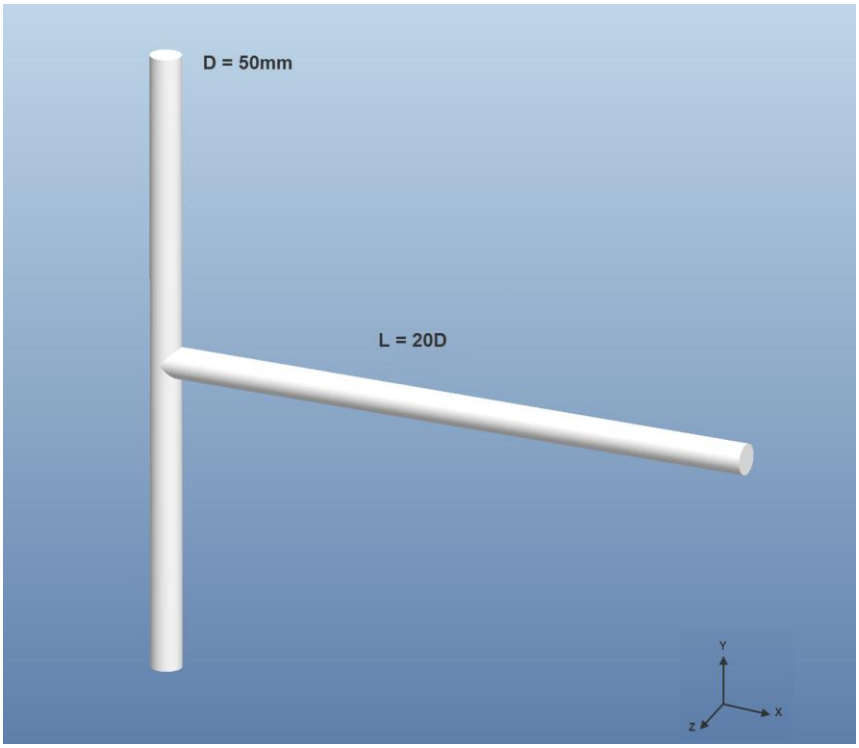

Figure 5.2 Domain with prolonged branch arm

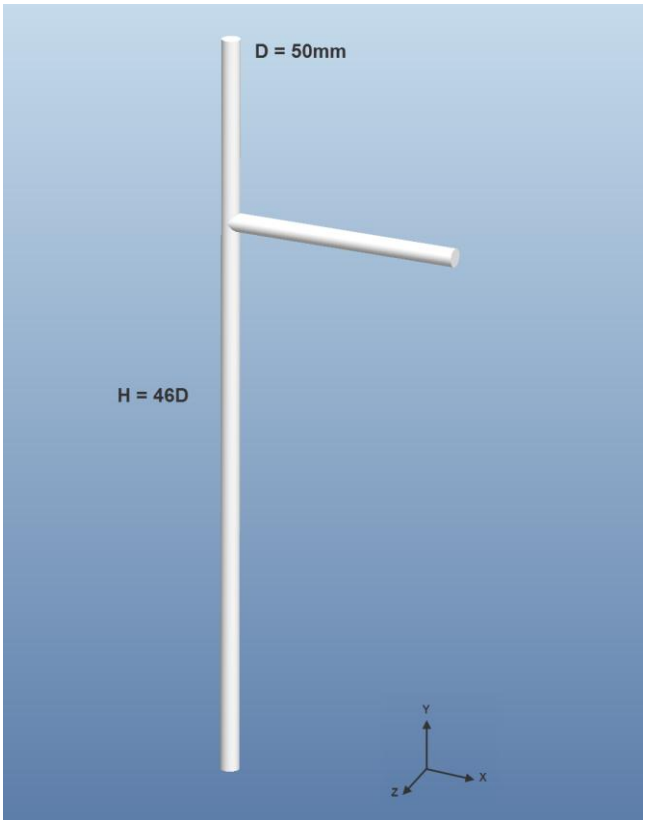

Figure 5.3 Domain with prolonged main arm

A block-structured meshing approach was used to create meshes with only hexahedral/quad cells. Refinements were made in the vicinity of the junction to resolve the rapid changes in the flow occurring there. The smallest elements were created at the wall to resolve boundary layers and the cell size increased by 10% in a radial direction. The distribution of cells at the inlet and around the junction can be seen in Figure 5.4. In addition to the meshes for the three domains, refined meshes were also created to investigate the influence of mesh size. Statistics for all the meshes can be found in Table 5.1.

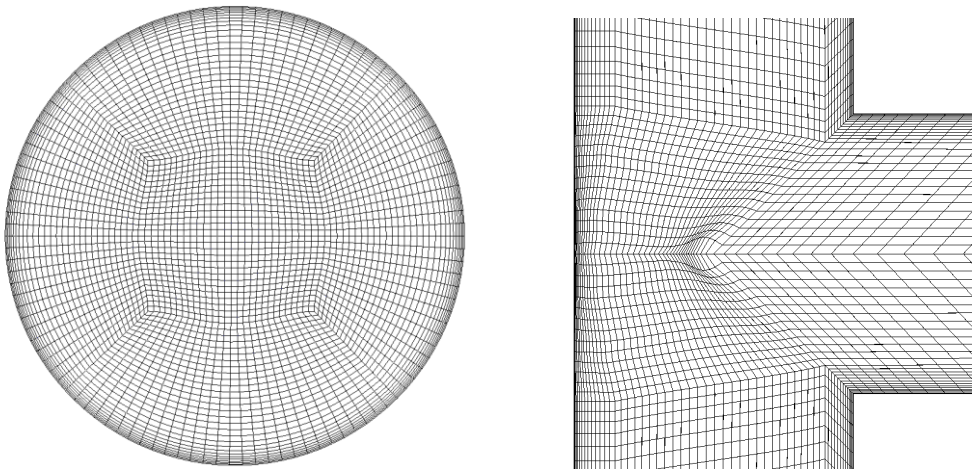

Figure 5.4 To the left: Element distribution at inlet. To the right: Zoom of mesh in vicinity of the junction.

Table 5.1 Mesh statistics

Mesh	Total no. of cells	Cell size near wall [mm]	Mean cell size [mm]	Max cell size [mm]	y^+
Original mesh	~150 000	0.3	11	14	20-60
Refined original mesh	~1 300 000	0.1	6	7	0-20
Prolonged mesh	~160 000	0.3	11	14	20-60
Refined prolonged mesh	~1 400 000	0.1	6	7	0-20
Mesh with separate inlets	~190 000	0.3	11	14	20-50

5.2 Simulation settings

Several combinations of settings were tested. Parameters were systematically changed in order to investigate their effect on the results. In the first part of the project the effect of dispersed phase diameter, turbulence model, drag law, discretising scheme for the gas volume fraction (GVF) equation, phase formulation and turbulence dispersion force was investigated. In the latter part, focus was on investigating the use of more advanced bubble/particle models.

CFX does not offer any specific discretising schemes for the GVF equation so the effect of this parameter was only investigated in Fluent. The choice of parameters was

based on settings presently used at Aker Solutions, recommended settings for the software used and settings commonly used for similar problems in open literature. In addition to the parameters previously mentioned, the effect of mesh size and steady state versus transient time formulation was investigated. Two meshes, a coarser and a refined, were used to investigate the influence of mesh size. Regarding time formulation, a steady state simulation is much less time consuming than a transient simulation so from a time cost perspective it is better to run steady state simulations. However, multiphase flows often exhibit transient behaviour and forcing a transient flow in to a steady state might produce an unphysical solution. A transient simulation was therefore run in each code to investigate the transient behaviour and to see if steady state simulations were justified.

For the simulations ran in Fluent the pressure-based coupled solver was used with gravity enabled. In CFX, the coupled solver with gravity enabled was used. The settings for the simulations in Fluent and CFX can be found in Table 5.2 and 5.3, respectively.

Table 5.2 Simulations done in Fluent

Run	Settings
First part of the project – Effect of changing parameters	
1.	**Steady State Eulerian** 2mm air bubbles Schiller-Naumann drag law Realisable k-ε turbulence model First order discretising schemes
2.	Changed bubble diameter: 70μm
3.	Changed bubble diameter: 4mm
4.	Changed phase formulation: 2mm water bubbles
5.	Changed drag law: Universal
6.	Changed turbulence model: Shear stress transport (SST)
7.	Changed discretising scheme for GVF-equation: HRIC (High resolution interface capturing)
8.	Added force: Turbulent dispersion
9.	Changed mesh: Refined

10.	Changed time formulation: Transient
11.	**Transient VOF** LES turbulence model First order discretising scheme for GVF-equation
12.	Changed turbulence model: k-ε
13.	Changed discretising scheme for GVF-equation: HRIC
Second part of the project – Investigation of bubble models	
14.	2 constant bubble diameters: 1mm and 0.1mm
15.	2 constant bubble diameters: 2mm and 0.1mm
16.	3 constant bubble diameters: 2mm, 1mm and 0.1mm
17.	IAC with sauter mean diameter
18.	PBM – Discrete Method Number of size bins: 7 Size interval: min. 1×10^{-7} m, max. 0.1m
19.	PBM – QMOM Inlet Moments 1 Size interval: min. 1×10^{-7} m, max. 0.1m
20.	PBM – QMOM with changed inlet moments Inlet Moments 2
21.	PBM – QMOM with changed dispersed phase size interval Size interval: min. 1×10^{-9} m, max. 0.1m
22.	PBM – QMOM with breakage and coalescence modelling
23.	PBM – Discrete with turbulent dispersion
24.	PBM – QMOM with turbulent dispersion

Table 5.3 Simulations done in CFX

Run	Settings
First part of the project – Effect of changing parameters	
1.	**Steady State Inhomogeneous** 2mm air bubbles Ishii-Zuber drag law

	k-ε turbulence model First order discretising schemes
2.	Changed bubble diameter: 70μm
3.	Changed bubble diameter: 4mm
4.	Changed phase formulation: 2mm water bubbles
5.	Change phase formulation: Both phases continuous
6.	Changed drag law: Schiller-Naumann
7.	Changed turbulence model: SST
8.	Added force: Turbulent dispersion
9.	Changed mesh: Refined
10.	Changed time formulation: Transient
11.	**Steady State Homogeneous**
Second part of the project – Investigation of bubble models	
12.	MUSIG Equal diameter size distribution and breakage/coalescence models Number of size bins: 7 Size interval: min. 1×10^{-7} m, max. 0.1m
13.	MUSIG with changed size distribution: Geometric
14.	MUSIG with changed size distribution: Equal mass
15.	MUSIG Geometric size distribution Changed size interval: min. 1×10^{-7} m, max. 0.05m
16.	MUSIG Equal mass size distribution Changed size interval: min. 1×10^{-7} m, max. 0.01m
17.	MUSIG Geometric size distribution With turbulent dispersion

Time step and under relaxation factors were changed only if necessary for obtaining convergence. This is described in more detail in Section 5.5.

5.3 Boundary conditions

The inlet velocity and volume fraction for the gas and liquid phase were known from the experimental study. For the outlets, the flow split for the bulk flow between the run and the branch was given. In the experiment, the overall flow split was controlled by varying the outlet pressures for the two pipes, but the pressure values were not stated in the article and therefore the bulk flow split was specified for the outlets in the simulations. However, for some simulations a pressure outlet condition had to be implemented to achieve convergence as the pressure outlet condition is more stable than the flow split condition. The values for the outlet pressures were then taken from a previously converged simulation and adjusted to obtain the correct bulk flow split. For the pipe walls a no slip condition was implemented.

Additional boundary conditions had to be specified when polydispersed modelling was implemented. Using the IAC model, a value for the interfacial area concentration at the inlet had to be specified. The default value in Fluent was used. With the discrete PBM in Fluent, values for the fraction of each size bin were defined and with the QMOM PBM values for the inlet moments had to be specified. As it might be difficult to estimate the inlet moments, two sets of moments were used to investigate the sensitivity of the solution to the inlet moments. The first set of inlet moments was estimated based on formulas given by Lundevall (2011). The second set of inlet moments was chosen arbitrarily. In CFX automatically generated values for the size bin fractions was used. A summary of the boundary conditions can be found in Table 5.4.

Table 5.4 Boundary conditions

Boundary	Condition
Inlet	$u_g = 5\,\text{m/s},\ u_l = 6.21\,\text{m/s},\ \alpha_g = 0.52$
Outlets	$\dot{m}_{branch} = 20\%, \dot{m}_{run} = 80\%$ or pressure outlet
Pipe walls	No slip
IAC	0.001 1/m

Bin fractions	$f_0 = 0.192$ $f_1 = 0.192$ $f_2 = 0.192$ $f_3 = 0.192$ $f_4 = 0.096$ $f_5 = 0.096$ $f_6 = 0.038$
Inlet Moment 1	$m_0 = 365625$ $m_1 = 730$ $m_2 = 1.4625$ $m_3 = 0.0002925$ $m_4 = 5.85 \times 10^{-6}$ $m_5 = 1.2 \times 10^{-8}$
Inlet Moment 2	$m_0 = 1 \times 10^{10}$ $m_1 = 1 \times 10^{6}$ $m_2 = 100$ $m_3 = 0.1$ $m_4 = 1 \times 10^{-4}$ $m_5 = 1.2 \times 10^{-8}$

5.4 Convergence criteria

Convergence was judged based on three criteria. First of all, the normalised equation residuals for momentum, continuity, turbulence and volume fraction equations were monitored and would desirably drop below $1e^{-5}$. However, this criterion alone is not enough for judging the validity of the solution. For some cases the residual criterion might never be fulfilled even though the solution is valid and for other cases the solution can be incorrect even though the residuals are low. Therefore, mass conservation and outlet pressures were also monitored. The fractional difference in mass flow in and out the domain should be less than 0.01% and the mass flow through the open boundaries as well as the pressure at each outlet should remain constant for a number of iterations if the simulation would be said to be converged.

5.5 Evaluation criteria

Results from a numerical simulation can be judged based on different criteria. A more complex model might produce accurate results for a very detailed level of information but often also implies long calculation times and/or numerical instabilities. What is judged as good results depends on the type of analysis that is to be made. For example, for a concept study a fast simulation yielding a basic understanding of the flow situation might be considered the best even though more accurate results might be produced with a more complex model. However, for a detailed study the accuracy of the simulations is probably more important than time requirement. To take all perspectives into account, the simulations were judged based on the following three conditions; accuracy, time requirement and numerical stability.

The criterion for time requirement was straightforward. If a simulation needed little time to converge it was judged as good with respect to time and vice versa for long calculation times. To judge the accuracy of the results, the prediction of known flow phenomena and/or known values/features was evaluated. For the third criterion, the numerical stability, evaluation was based on how difficult it was to obtain a converged solution. If it was needed to reduce under relaxation factors and/or use other methods for stabilising the solution to achieve convergence the simulation was judged as less good with respect to stability.

6 Results and Discussion

In this section, the results from the simulations are presented and compared with experimental data. In Section 6.1 the prediction of the phase separation phenomenon is discussed. The predicted global and local parameters are compared to experimental data in Section 6.2 and 6.3, respectively. In Section 6.4 – 6.6 results from simulation done in different codes and with different parameters are presented and discussed. Finally, a discussion about convergence issues and possible error sources can be found in Sections 6.7 and 6.8, respectively.

6.1 Phase separation phenomenon

Figure 6.1 shows a representative contour plot of static pressure in vicinity of the junction. The pressure is high at the downstream corner of the junction and low at the leading edge corner. The air phase is lighter and possesses less inertia than the water phase and thus responses easier to the local pressure gradient at the junction. Consequently, a higher proportion of gas is drawn into the branch arm. This phenomenon is further illustrated by the velocity vector plot in Figure 6.2 where the air velocity vectors are coloured by grey and the water vectors are coloured by black. It is evident from Figure 6.2 that the air phase turns more abruptly away from the high pressure corner than the water phase. This creates a slip velocity between the phases and is a condition for the phases to be able to separate in the branch arm.

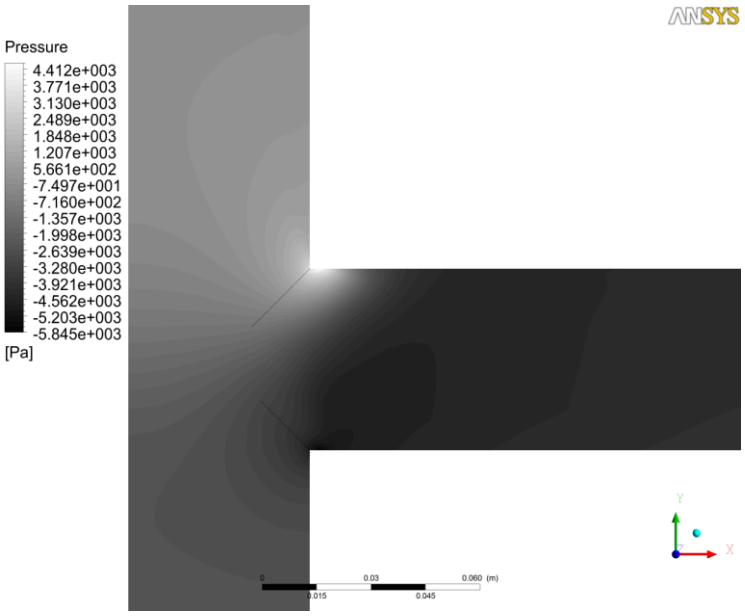

Figure 6.1 Contour plot of static pressure on mirror plane z = 0, CFX Run 1.

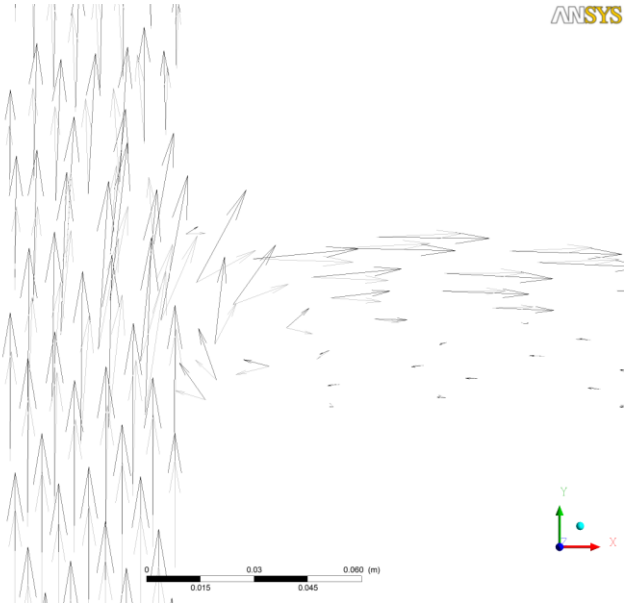

Figure 6.2 Velocity vector plot on mirror plane z = 0, CFX Run 1. Air vectors are coloured by grey and water vectors are coloured by black.

Figure 6.3 shows representative contours of gas volume fraction for the Eulerian/inhomogeneous models in Fluent and CFX. Figure 6.4 shows corresponding contour plots for the VOF/homogeneous models. By comparison of the results from

the simulations done using a two-fluid model with the results from simulations using a VOF/homogeneous approach it is clearly seen that the homogenous approach is not suitable for this type of application. Since the phases are mixed at the inlet, the assumption that the phases have a shared velocity field results in that separation never occurs and instead an almost homogeneous mixture with 50% air and 50% water flows through the entire junction. Using a two-fluid model, the phase split phenomenon that occurs in a branching T-junction is clearly captured with both codes. A higher proportion of gas is diverted into the side branch and a gas pocket occurs in the lower part of the branch arm in the vicinity of the junction. This is in consistency with the experimental results by Fungatamasan and Davis (1990) as well as several other experiments concerning phase redistribution in T-junctions (Mudde, Groen and Akker 1993, Walters, Soliman and Sims 1998 and Elazhary 2012).

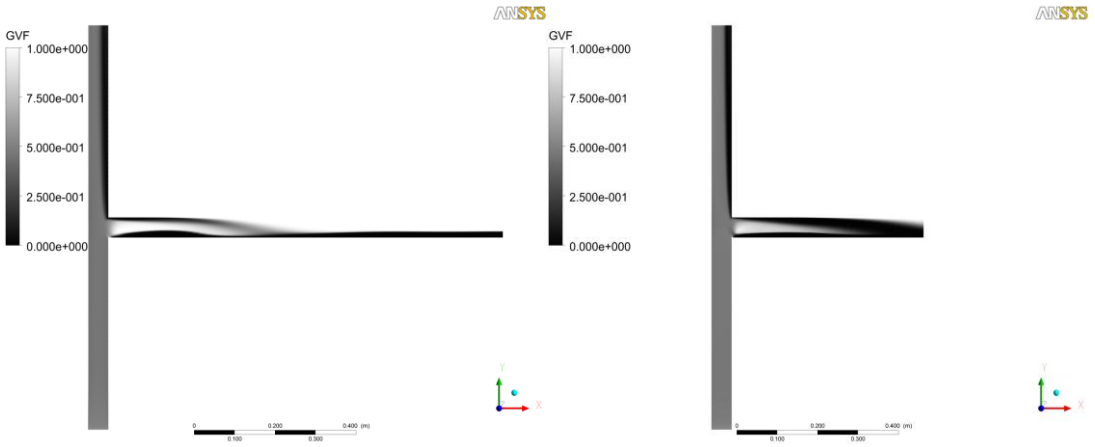

Figure 6.3 Contour plots of volume fraction on mirror plane z = 0. To the left: Fluent Run 1. To the right: CFX Run 1.

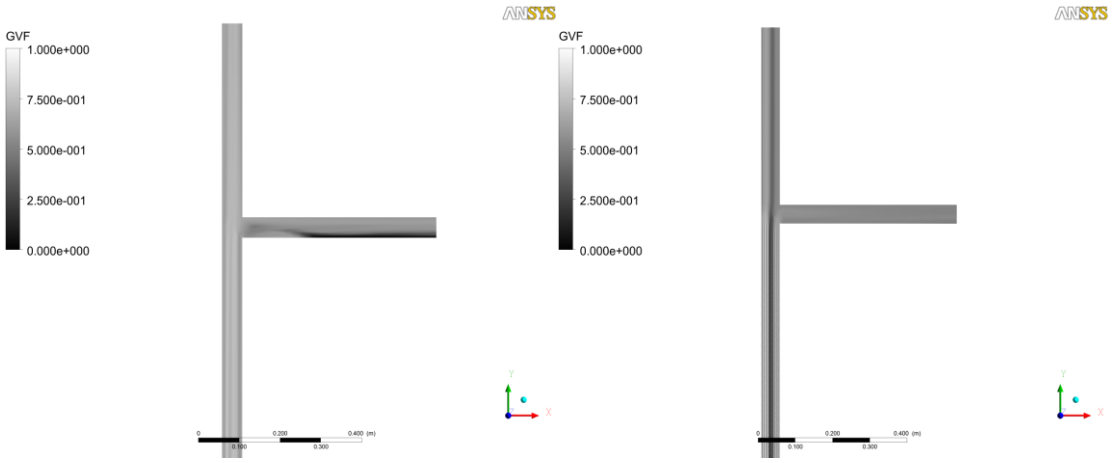

Figure 6.4 Contour plots of volume fraction on mirror plane z = 0. To the left: Fluent Run 10. To the right: CFX Run 10.

In Figure 6.5, contours of velocity ratio between the gas phase and the liquid phase is shown. It can be seen that in most parts of the junction, the velocity ratio is almost at unity, meaning that the air and the water travels at the same speed. However, just at the junction and in the lower part of the branch arm directly afterwards the gas travels faster than the water. This is in consistency with the fact that the gas phase possesses lower inertia and therefore is easier rushed into the side branch.

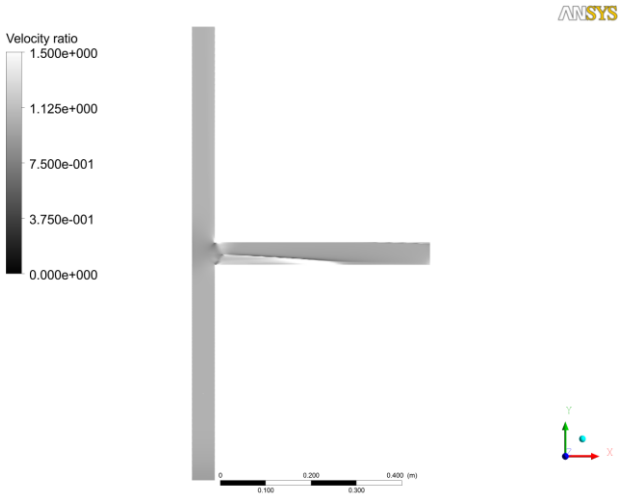

Figure 6.5 Representative contour plot of velocity ratio on mirror plane z=0, CFX Run1.

6.2 Prediction of global parameters

In Table 6.1 the predicted values for volume fraction and mixture velocity in the run and branch arms are presented and compared to the experimental data. The global volume fraction at the outlets is predicted fairly well for most of the settings and shows the same trend as in the experiment. However, the averaged velocity at the outlets differs from the experiment. The velocity at the branch outlet is generally under predicted and vice versa for the run outlet. The reason for this erroneous prediction is not clear, however, the same issue has been found in simulations done for a similar setup by Oliveira (1992). Adding models for polydispersed flow generally improved agreement with the experimental data, especially for the velocity fields. Without polydispersed modelling the volume fraction is best predicted in Fluent with the SST turbulence model (Run 6) or the refined mesh (Run 9). However, the velocity in the branch arm is under predicted with more than 30% for both of these settings. The velocities are most accurately predicted using the discrete PBM (Run 18) in Fluent, however, the best overall agreement was obtained using the QMOM PBM in Fluent (Run 19) or the MUSIG model with geometric size distribution and changed size interval in CFX (Run 15).

Table 6.1 Comparison between predicted global parameters and experimental data

Run	$\sigma_s = \dot{m}_{g,3} / \dot{m}_{g,1}$	α_{branch}	$u_{m,branch}$[m/s]	α_{run}	$u_{m,run}$[m/s]
Exp. Study	0.60	0.77	2.74	0.35	3.41
Fluent Run1	0.43	0.69	1.79	0.36	3.72
Fluent Run2	0.20	0.46	1.11	0.48	4.46
Fluent Run3	-	-	-	-	-
Fluent Run4	0.41	0.65	1.70	0.37	3.83
Fluent Run5	-	-	-	-	-
Fluent Run6	0.41	0.76	1.74	0.37	3.83
Fluent Run7	-	-	-	-	-
Fluent Run8	0.41	0.65	1.74	0.38	3.82
Fluent Run9	0.43	0.76	1.64	0.35	3.81

Fluent Run10	0.41	0.68	1.67	0.35	3.80
Fluent Run11	0.18	0.63	1.27	0.51	5.03
Fluent Run12	-	-	-	-	-
Fluent Run13	-	-	-	-	-
Fluent Run14	0.34	0.52	1.74	0.43	3.89
Fluent Run15	0.29	0.55	1.57	0.43	4.16
Fluent Run16	0.27	0.48	1.41	0.45	4.18
Fluent Run17	0.65	0.76	2.26	0.23	3.26
Fluent Run18	0.64	0.75	2.31	0.22	3.22
Fluent Run19	0.41	0.68	2.26	0.37	3.83
Fluent Run20	0.31	0.61	1.81	0.41	4.14
Fluent Run21	0.41	0.68	2.26	0.37	3.83
Fluent Run22	0.35	0.68	2.00	0.39	4.01
Fluent Run23	-	-	-	-	-
Fluent Run24	0.41	0.63	1.72	0.38	3.82
CFX Run1	0.32	0.61	1.45	0.41	4.17
CFX Run2	0.24	0.44	1.19	0.44	4.45
CFX Run3	0.37	0.65	1.66	0.38	4.00
CFX Run4	-	-	-	-	-
CFX Run5	0.31	0.61	1.43	0.41	4.17
CFX Run6	0.32	0.66	1.46	0.40	4.20

CFX Run7	0.31	0.62	1.48	0.41	4.17
CFX Run8	0.32	0.59	1.49	0.41	4.11
CFX Run9	0.31	0.67	1.41	0.41	4.20
CFX Run10	0.32	0.60	1.46	0.41	4.15
CFX Run11	0.20	0.50	1.16	0.51	4.36
CFX Run12	0.43	0.75	1.97	0.35	3.83
CFX Run13	0.70	0.77	2.78	0.20	3.04
CFX Run14	0.81	0.80	2.92	0.15	2.81
CFX Run15	0.51	0.79	2.43	0.30	3.50
CFX Run16	0.42	0.67	1.85	0.35	3.81
CFX Run17	0.54	0.77	2.17	0.30	3.48

6.3 Prediction of local distributions

Fungtamasan and Davis (1990) measured the local distribution of volume fraction and gas velocity along four lines at cross sections 500 mm from the junction; along the y-axis and along the z-axis in the middle of the branch arm and along the x-axis and the z-axis in the middle of the run arm, these lines are marked in Figure 6.6. In Figures 6.7 – 6.10 and 6.11 – 6.14 representative predicted local distributions of volume fraction and gas velocity are shown and compared to the experimental data. The agreement is generally low for both the volume fraction and the velocity.

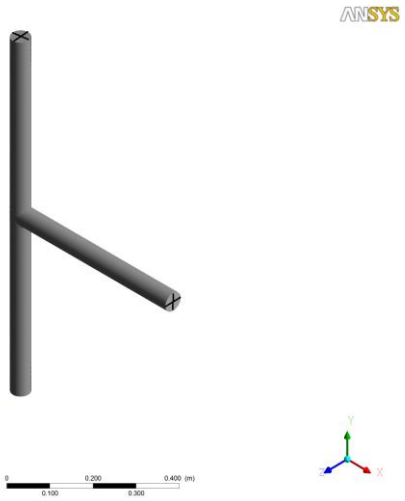

Figure 6.6 Definition of lines at which the local distributions of mixture velocity and volume fraction have been measured

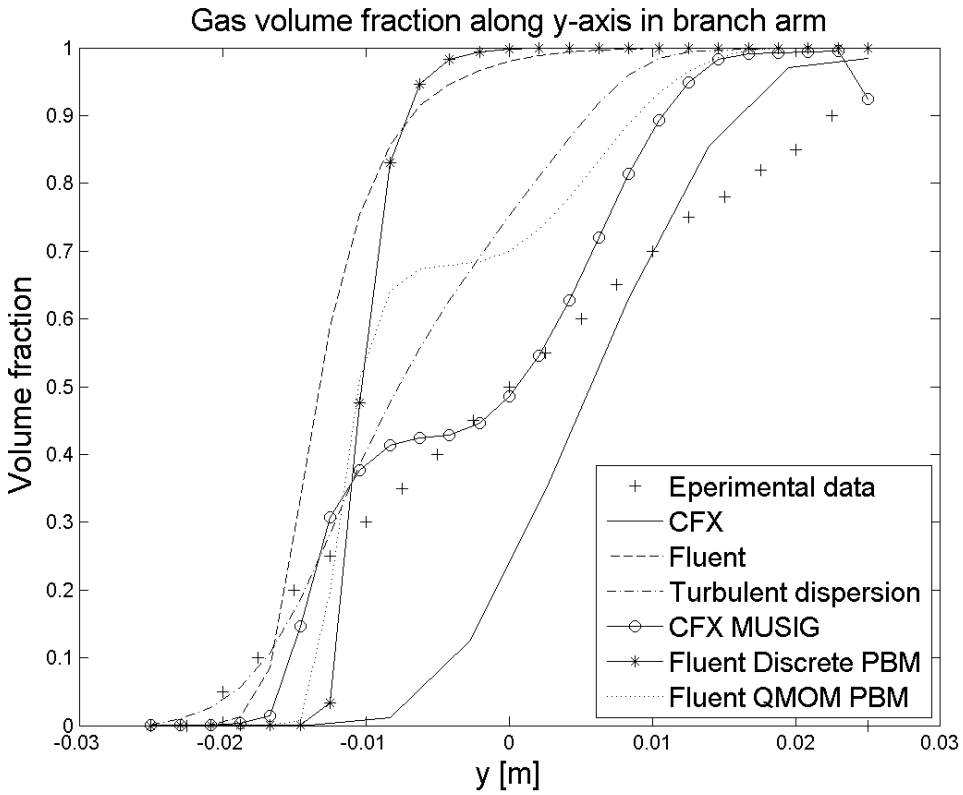

Figure 6.7 Gas volume fraction along y-axis in branch arm

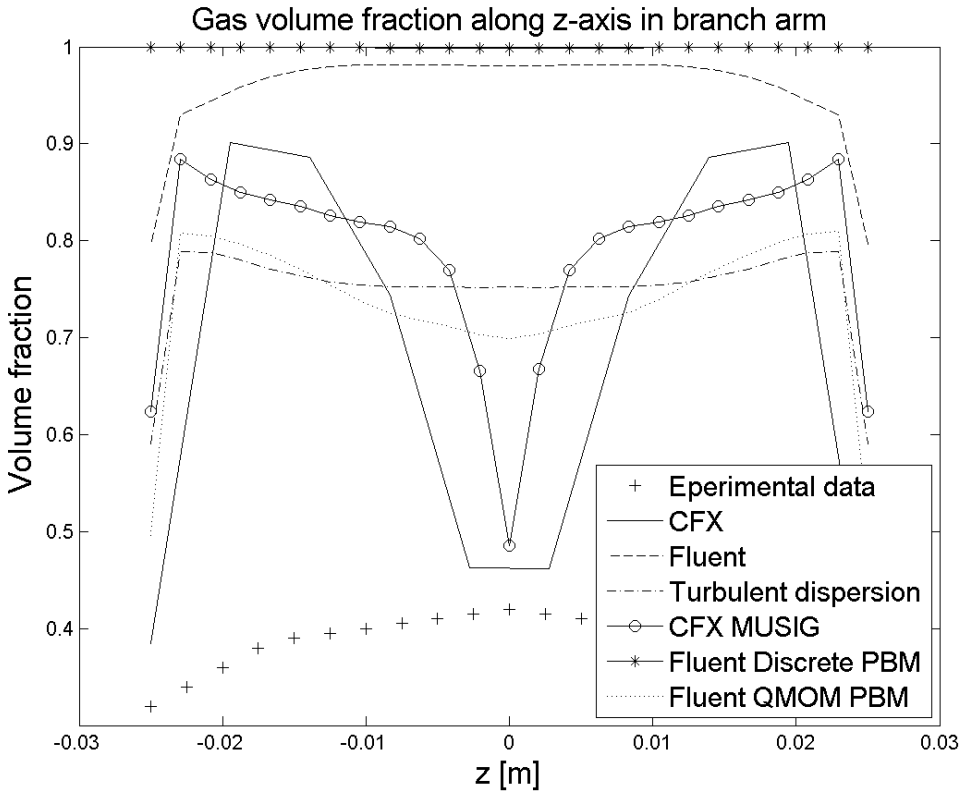

Figure 6.8 Gas volume fraction along z-axis in branch arm

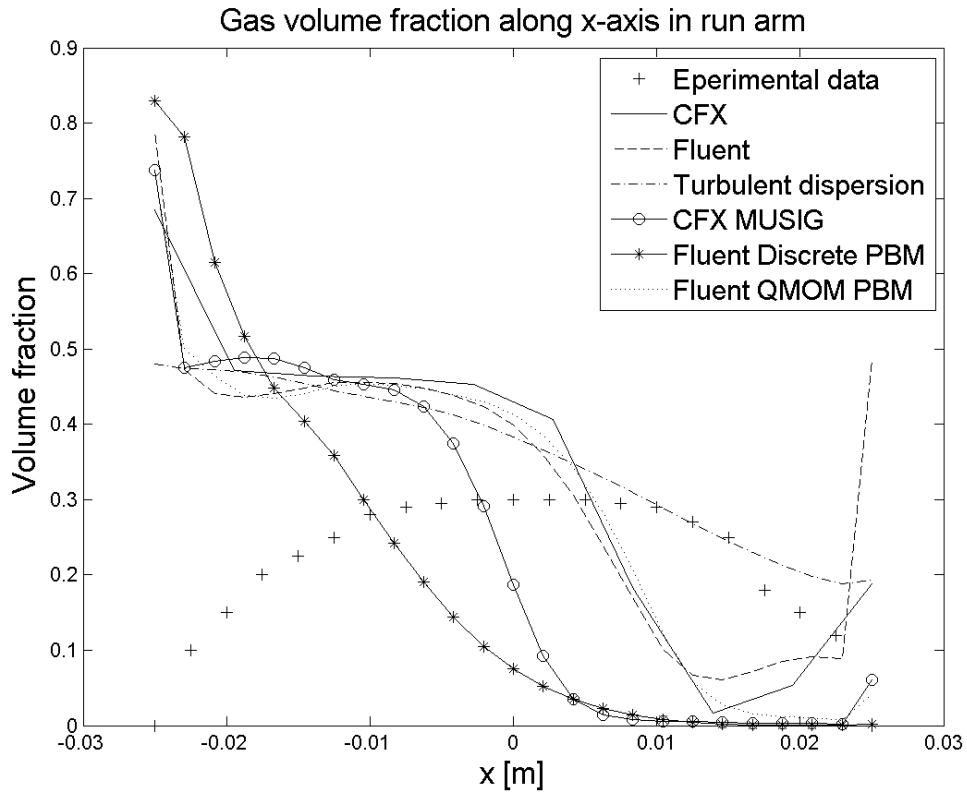

Figure 6.9 Gas volume fraction along x-axis in run arm

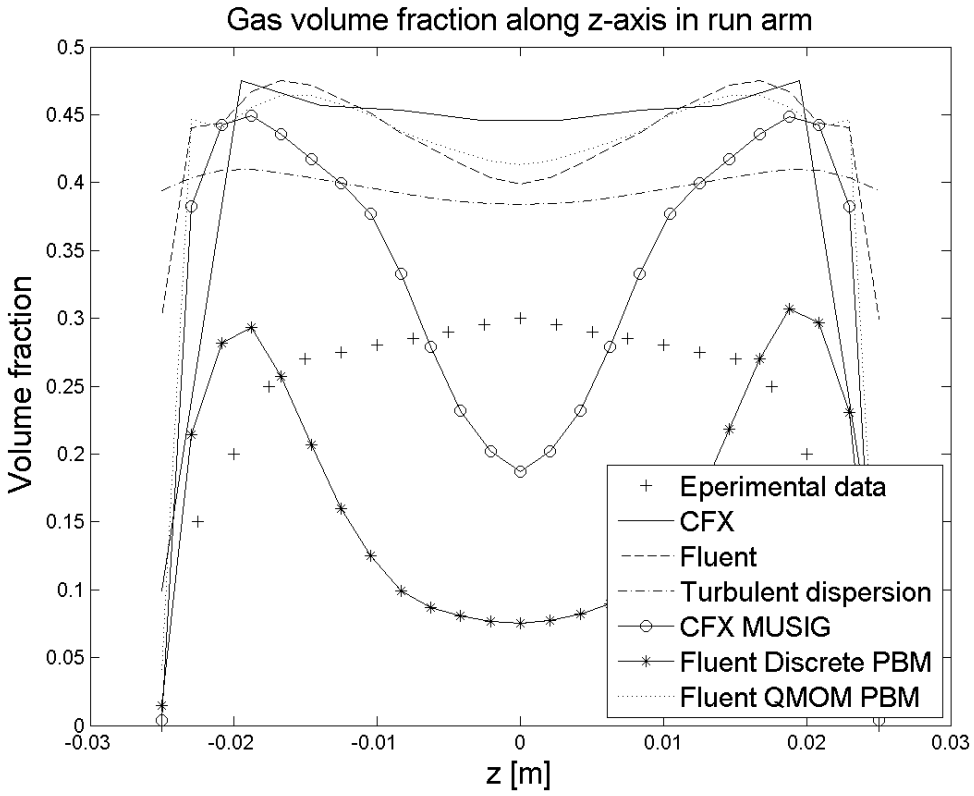

Figure 6.10 Gas volume fraction along z-axis in run arm

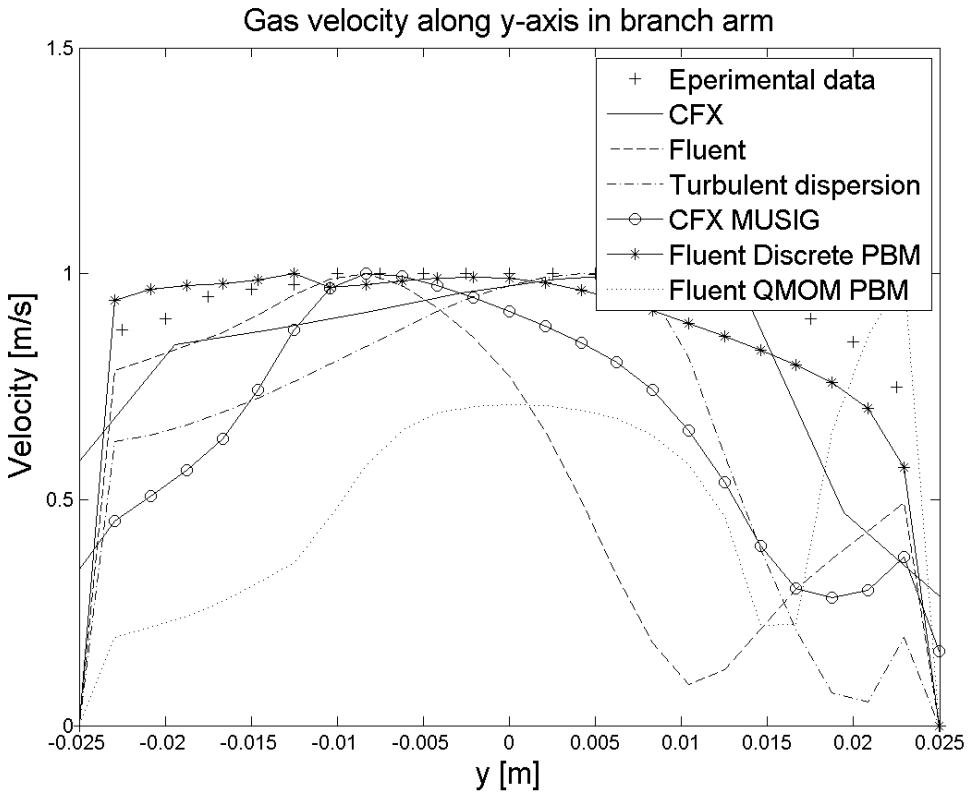

Figure 6.11 Normalised gas velocity along y-axis in branch arm

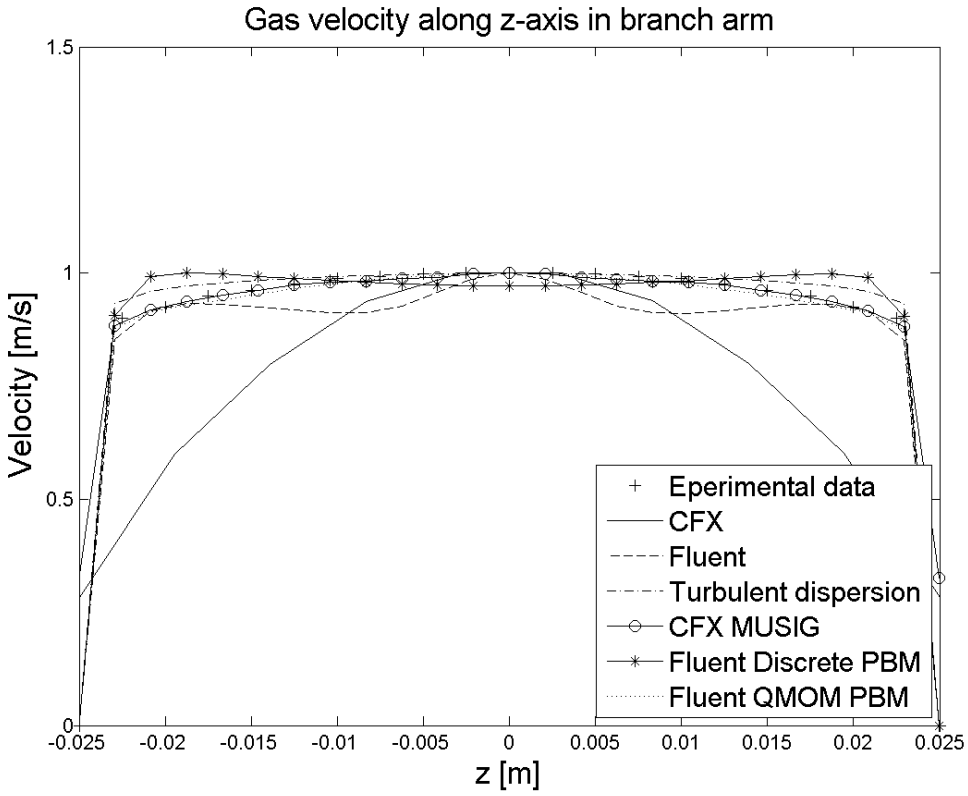

Figure 6.12 Normalised gas velocity along z-axis in branch arm

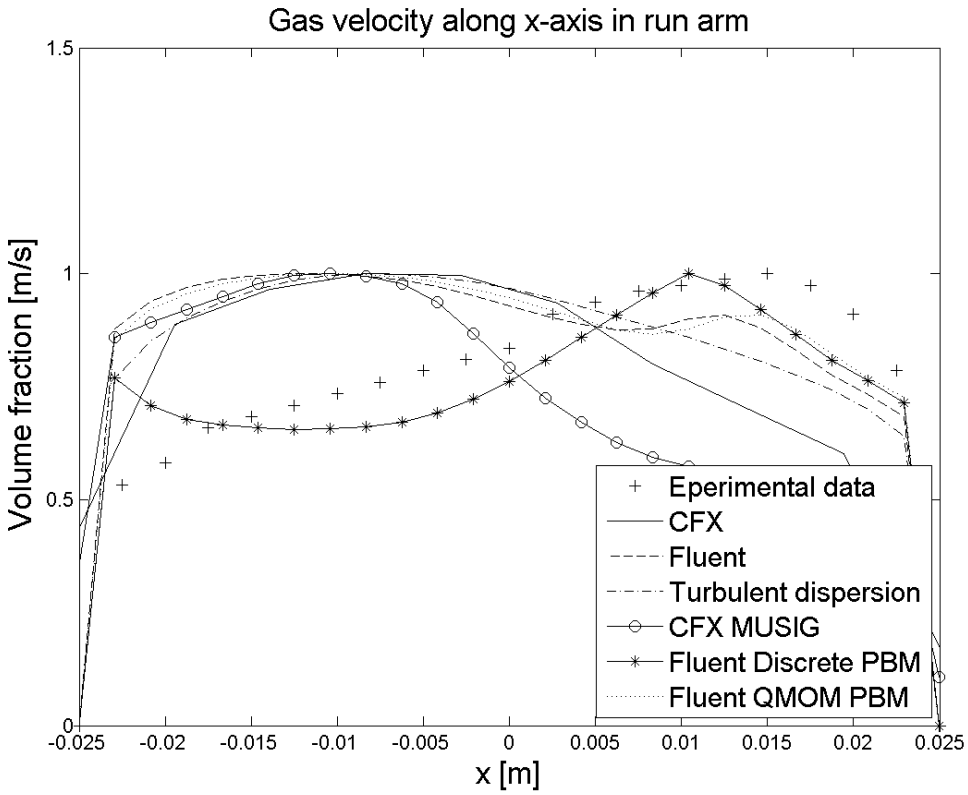

Figure 6.13 Normalised gas velocity along x-axis in run arm

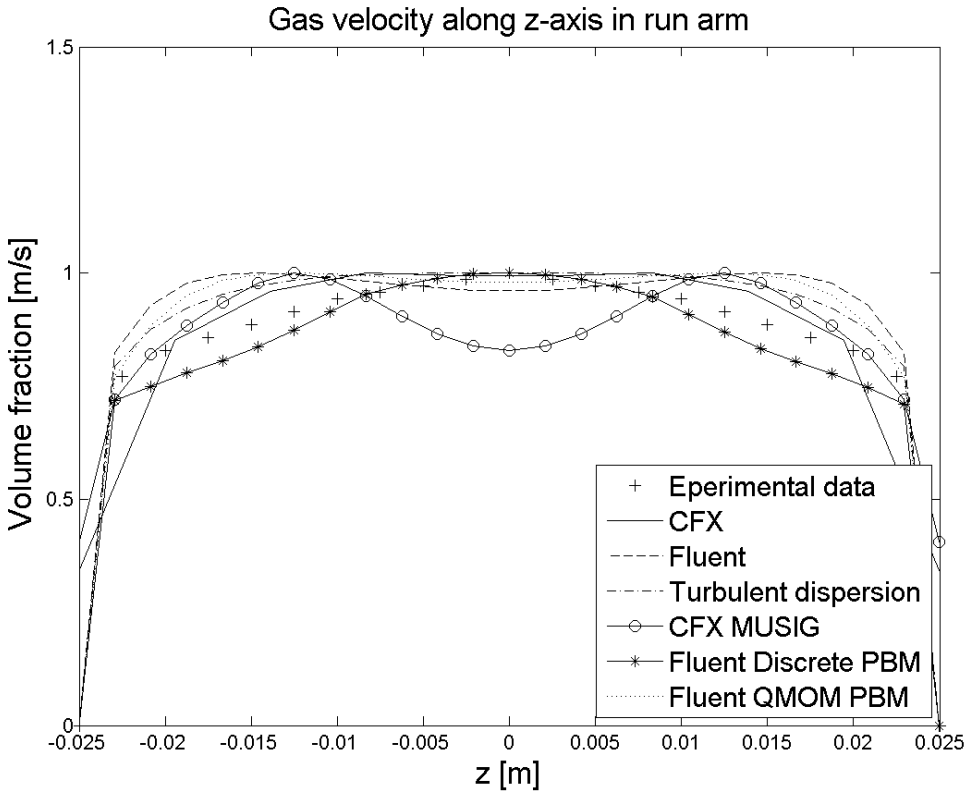

Figure 6.14 Normalised gas velocity along z-axis in run arm

The predicted distributions of volume fraction along the y-axis in the branch arm show the same trend as the experimental data, with a higher concentration of gas in the upper part of the branch, however, as can be seen in Figure 6.7 the predicted separation is generally stronger than in the experiment. Along the z-axis, both in the run arm and in the branch arm, the predicted volume fraction differs quite drastically both from the experiment and depending on the solver/settings, see Figure 6.8 and Figure 6.10. The large differences depending on solver and settings are due to local peaks and dips along lines in the cross section. This phenomenon can be seen in Figure 6.15 in Section 6.4, which shows contours of volume fraction on cross sections in the branch arm. As data is taken at points on four straight lines any singularities will have a large effect on the volume fraction/velocity profiles and the large dips in Figure 6.8 and Figure 6.10 might not be representative for the solution.

The largest deviation from the measured volume fraction can be identified along the x-axis in the run arm, see Figure 6.9. Using CFD, a gas free zone is predicted along the run arm side above the branch for most cases. The gas free zone can be seen also in the contour plots of volume fraction, see for example Figure 6.3. In the experiment, only a slight decrease in gas volume fraction was measured at this side of the run arm. As can be seen in Figure 6.9, adding a turbulent dispersion force decreases the gas free zone and the distribution of volume fraction is in better consistency with the experimental data. A more thorough discussion about the effect of adding the turbulent dispersion force is given in Section 6.5.6.

Both in the branch arm and in the run arm, the predicted profiles of gas velocity along the z-axis generally show the same trend as in the experiment and if all the data is normalised with the maximum velocity the agreement between experimental and predicted values is very good. Along the y-axis in the branch arm, the predicted velocity profiles above all differ from the experimental data in the upper part of the arm. With most settings, the velocity decreases quite rapidly in the upper, gas rich, part of the branch arm with a small peak in gas velocity near the upper wall. This can be seen in Figure 6.11. The reason for this deviation is not clear. An exception is once again the gas velocity profile predicted using the discrete PBM in Fluent, which instead shows a quite good agreement with the experimental data.

Just as regarding gas volume fraction, the largest deviation from the experimental data is identified along the x-axis in the run arm. Fungtamasan and Davis (1990) found that the gas velocity along this line was at its lowest near the wall opposite from the junction and then increased towards the other side. Without any model for polydispersed flow, the predicted velocity profiles are almost mirrored compared with the experimental data. Adding polydispersed modelling resulted in a small peak in velocity near the branch side of the wall, although not near the same magnitude as in the experiment. The only setting resulting in a distinct increase in velocity near the right-most side of the outlet was with the discrete PBM in Fluent. One might suspect that the erroneous prediction of the gas velocity profile is related to the erroneous prediction of the gas free zone in the run arm. However, it is interesting to note that the largest gas free zone is predicted using the discrete PBM, which actually is in best agreement with the experimental data regarding velocity. A reason for the inaccurate prediction might be that only drag force, and for some cases also turbulent dispersion force, is considered when modelling the interphase transfer. There is a risk that this simplification means that forces that in reality have a large impact on the flow phenomena in the junction are neglected.

6.4 Comparison between Fluent and CFX

As previously noted, the phase redistribution phenomenon is captured with both codes and the contours of volume fraction on the mirror plane show a similar shape for both CFX and Fluent, see Figure 6.3. However, Figure 6.15 shows contours of volume fraction on cross sections in the branch arm and in this plot one can see that the solutions show a similar behaviour although there are clearly differences in result using the two codes.

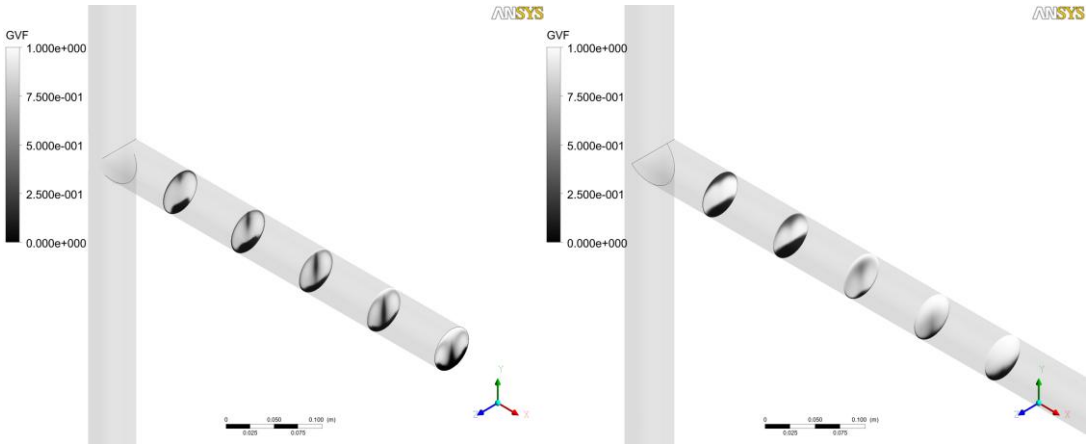

Figure 6.15 Contour plots of volume fraction at planes located at x = 0.1, 0.2, 0.3, 0.4, and 0.5. To the left: Fluent Run 1. To the right: CFX Run 1.

By comparing the results from simulations done in Fluent and CFX with the experimental data one can see that Fluent generally predicts the phase separation and velocities better than CFX for the given simulation settings. In addition to producing more accurate results, Fluent also has a larger number of models/parameters available than CFX making it easier for the user to customise the solver depending on the flow case. However, the simulations ran in CFX were generally more stable and needed fewer iterations to converge.

6.5 Effect of changing simulation parameters

Looking at the results in Table 6.1, it is evident that some of the parameters have a strong influence on the outcome of the simulations while others only have a weak effect. In this section, the effect of each parameter will be discussed.

6.5.1 Dispersed phase diameter

The parameter that has the strongest effect on the results is the dispersed phase diameter. When the diameter is increased from 2mm to 4mm the phase separation is also increased. The air recirculation zone in the lower part of the branch arm is elongated towards the outlet and more air is diverted in to the branch. When the diameter instead is decreased to 70μm the opposite occurs and the separation effect of the junction is lowered. These findings are in consistency with other numerical studies

concerning T-junctions (Issa and Oliveira 1993, Liu and Li 2011 and Oliveira 1992) and the effect was also clear using both programmes. When the dispersed phase diameter is increased the drag coefficient is lowered and the lighter gas phase responds more easily to the local pressure gradient in the junction and more gas is consequently diverted in to the side branch. In addition to increasing the separation effect in the T-junction, the increase in particle diameter also results in higher numerical instabilities. Compared to the simulations done with smaller diameter, the simulations with 4mm bubbles were much harder to converge. In CFX, the simulation with 4mm bubbles needed roughly twice as many iterations to converge compared to simulations with 2mm particles even though the results from the latter simulation was used as an initial guess. In Fluent, the simulation with the larger bubbles resulted in highly oscillatory residuals and did not converge even though running for several thousand iterations. In Figure 6.16 contours of volume fraction for the simulation with 70µm air bubbles can be seen to the left and for the simulation with 4mm air bubbles to the right.

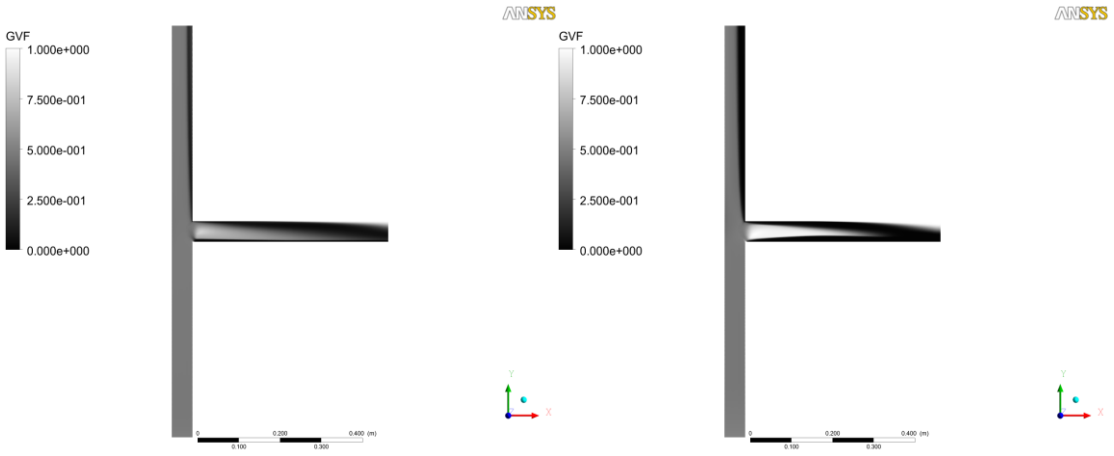

Figure 6.16 Contour plots of volume fraction on mirror plane z = 0. To the left: CFX Run 2 (with 70 µm bubbles). To the right: CFX Run 3 (with 4mm bubbles).

6.5.2 Phase formulation

A slight effect on the results can be seen for the simulations done with a changed phase formulation, especially in Fluent. Setting the water phase as the dispersed phase in Fluent changes the results slightly, around 5 % for the global parameters. Changing the dispersed phase affects the interphase drag as the drag is calculated based on the dispersed phase and air bubbles in water have other physics than water droplets in air

so the fact that the solution changes is quite expected. However, for many cases, such as the one analysed in this thesis, the choice of the dispersed phase is not straightforward and it is important to keep the effect of this formulation in mind. When using a continuous formulation for both phases in CFX the predicted global parameters and local distributions are very similar to those predicted with 2mm air bubbles, see Table 6.1.

Changing material for the dispersed phase above all affected the stability. Choosing the heavier phase as the dispersed phase resulted in high numerical instabilities and achieving convergence was troublesome. In Fluent, convergence was obtained only with a previously converged solution as initial guess and with low under-relaxation factors and in CFX convergence was not achieved at all.

6.5.3 Turbulence model

In CFX, the effect of changing turbulence model is very modest. In Fluent, the effect is somewhat stronger and the change in global parameters is roughly 5-10% when the SST turbulence model is used instead of the k-ε model. Figure 6.17 shows contours of volume fraction for the simulation done in Fluent with the SST model. By comparing Figure 6.17 with Figure 6.3, the largest difference between the two cases can be identified at the location of the gas pocket in the branch arm directly after the junction. When the SST turbulence model is used the gas pocket starts directly from the lower part of the branch arm instead of having a layer of water at the bottom, which is the case when the k-ε model is used. The gas pocket is also elongated towards the branch outlet. The SST turbulence model is known to perform better than the k-ε model in regions with adverse pressure gradients and separation (ANSYS Fluent Theory Manual 2011), which are phenomena that are present in the junction and this suggests that the solution obtained with the SST model is closer to the reality. However, it is important to remember that the same mesh has been used for the simulations with both turbulence models and these models have different mesh requirements (ANSYS Fluent Theory Manual 2011). Therefore, one should not draw too deep conclusions about which turbulence model that is superior for this application merely from these simulations. Since no data is given for this part of the junction in the experimental article it is not possible to determine which of the contours that is closest to the reality, but from the predicted global parameters one can

conclude that the volume fraction is better predicted compared with experimental data when the SST model is used.

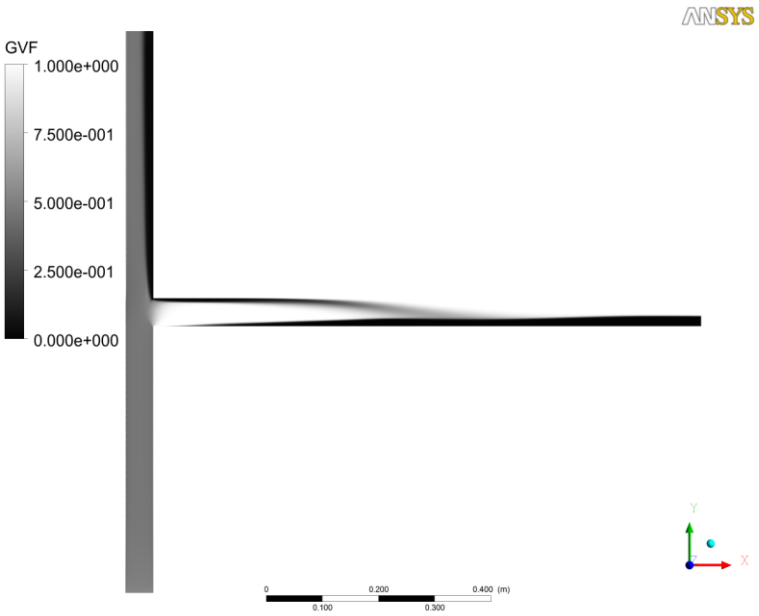

Figure 6.17 Contour plot of volume fraction on mirror plane z = 0, Fluent Run 6.

6.5.4 Discretisation scheme for volume fraction equation

The choice of discretising scheme for the volume fraction equation has a large impact on the numerical stability. When changing from the first order discretisation scheme to the HRIC discretisation scheme in Fluent, which theoretically should be better at retaining a sharp interface between the phases (ANSYS Fluent Theory Guide 2011), the residuals and the mass flow at the outlets showed a highly oscillating behaviour. No discussion can be made regarding the accuracy of the two discretisation schemes as the simulation done with the HRIC scheme did not converge.

6.5.5 Drag law

Changing the drag law does not affect the results in any major way, only a slight increase in volume fraction in the branch is noticed, but it greatly affects the convergence behaviour and numerical stability of the simulations in both CFX and

Fluent. The stability of the same scheme used in the different programmes also differs drastically. The use of the Schiller-Naumann drag law in Fluent resulted in rather stable simulations but when changing to the universal drag law, recommended for bubbly flow in the Fluent theory guide (2011), convergence was not obtained. In CFX, the use of the Schiller-Naumann drag law resulted in less stable simulations with oscillatory residuals and needed a good initial guess to converge. With the Ishii-Zuber drag law for interphase momentum transfer formulation, which is recommended for bubbly flow in the CFX theory guide (2011), the simulations were stable and generally converged within some hundred iterations.

6.5.6 Turbulent dispersion

Adding a turbulent dispersion force above all affects the solution by decreasing the separation of water in the run arm. This can be seen in Figure 6.18, showing contours of volume fraction for the turbulent dispersion case.

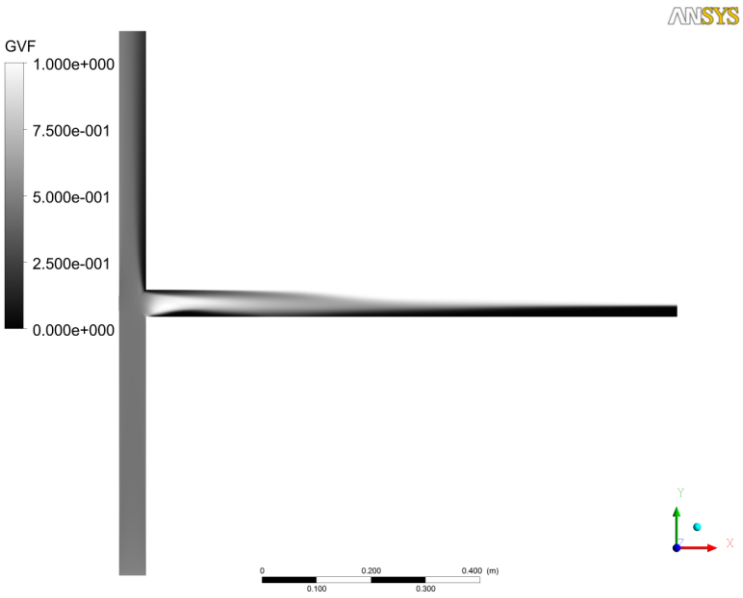

Figure 6.18 Contours of volume fraction on mirror plane z=0, Fluent Run 8.

Including the turbulent dispersion force changes the particle residence time in the domain and influences the drag force acting on the particles. As can be seen in Figure 6.18 the gas free zone is concentrated to an area in the run directly above the entry to the branch arm. Instead of being elongated towards the run outlet as in the case of no turbulent dispersion force, the separation effect is weakened along the run arm. This

phenomenon has been identified in several other experiments concerning T-junction (Mudde, Groen and van den Akker 1993, Saba and Lahey 1984). The phase redistribution in the branch is also effected when the turbulent dispersion force is added. The gas recirculation zone is shortened towards the junction and the stratification of the phases is delayed towards the branch outlet. This is also in better consistency with the experimental data which suggests that turbulent dispersion has a non-negligible effect on the phase distribution for this application. However, the averaged values of volume fraction and velocity are actually in slightly lower agreement with experimental data when the turbulent dispersion force is included.

Stability and convergence behaviour were also affected when the turbulent dispersion force was included in the solution. In Fluent, the convergence rate was slower but the residuals as well as outlet pressure and mass flow were stable when the turbulent dispersion force was added without any polydispersed model. However, with both polydispersed modelling and turbulent dispersion modelling, the solutions showed higher numerical instabilities. With the discrete PBM and the turbulent dispersion force included, convergence was not obtained. With the QMOM PBM convergence could be obtained, although with a slow convergence rate. Just as in Fluent, the convergence rate was slower in CFX when turbulent dispersion was taken into account. The stability was not affected to any greater extent.

6.5.7 Mesh size

In Figure 6.19 a contour plot of volume fraction for the case with the refined mesh is shown and in Figures 6.20 and 6.21 local distributions of volume fraction and gas velocity for the case with the coarse mesh and with the refined mesh are compared. Comparing the results from the two cases one can conclude that the results only changes slightly when the refined mesh, with approximately 9 times more elements than the coarser mesh, is used. For both codes the averaged gas volume fraction at the branch outlet increased by almost 10% compared to the more coarse mesh and is in better consistency with the experimental data. However, the predicted velocities are actually in lower agreement with the experimental data for the refined mesh although the difference is very modest for the two meshes. The fact that the solution changes when the finer mesh is used indicates that the solution is mesh dependent. However, since the change is rather small the simulations done with the coarser mesh can be

used to draw conclusions about the phenomena occurring in the junction. The choice of mesh for Euler-Euler simulations is not straightforward as the mesh length scale should be significantly larger than the dispersed phase diameter for the averaging to be correct, meaning that it is not possible to refine the mesh too much. A more detailed discussion about mesh dependency and mesh requirements is given in Section 6.8.

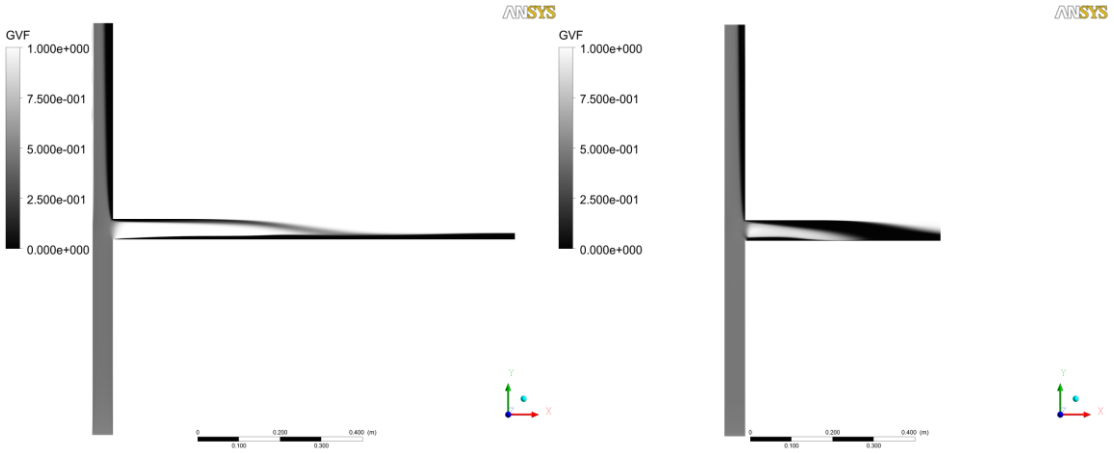

Figure 6.19 Contour plots of volume fraction on mirror plane z = 0. To the left: Fluent Run 9. To the right: CFX Run 9.

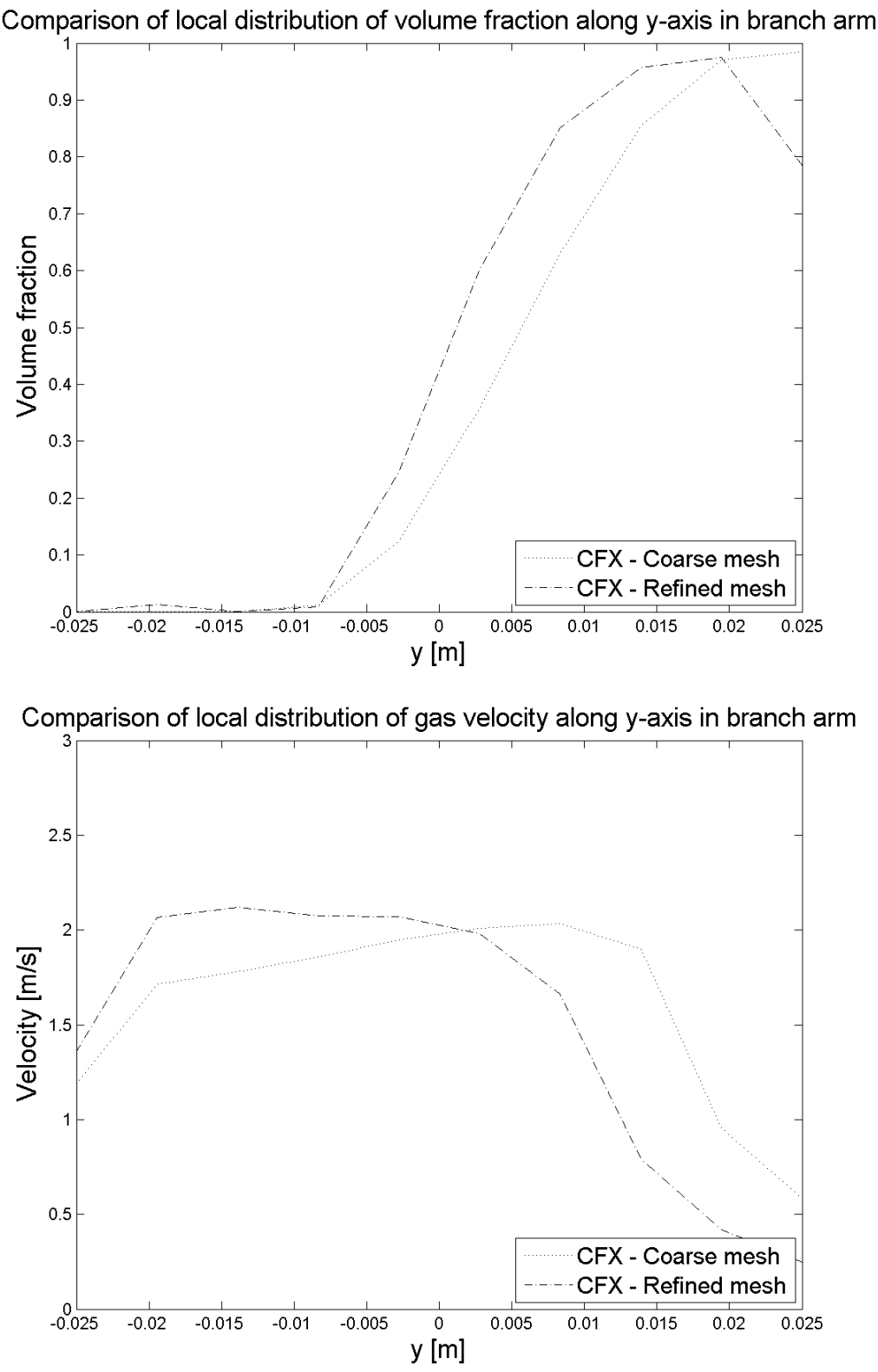

Figure 6.20 Comparison of local distributions along y-axis in branch arm for simulation with coarse and refined mesh. Uppermost: Local distribution of volume fraction. Bottommost: Local distribution of gas velocity.

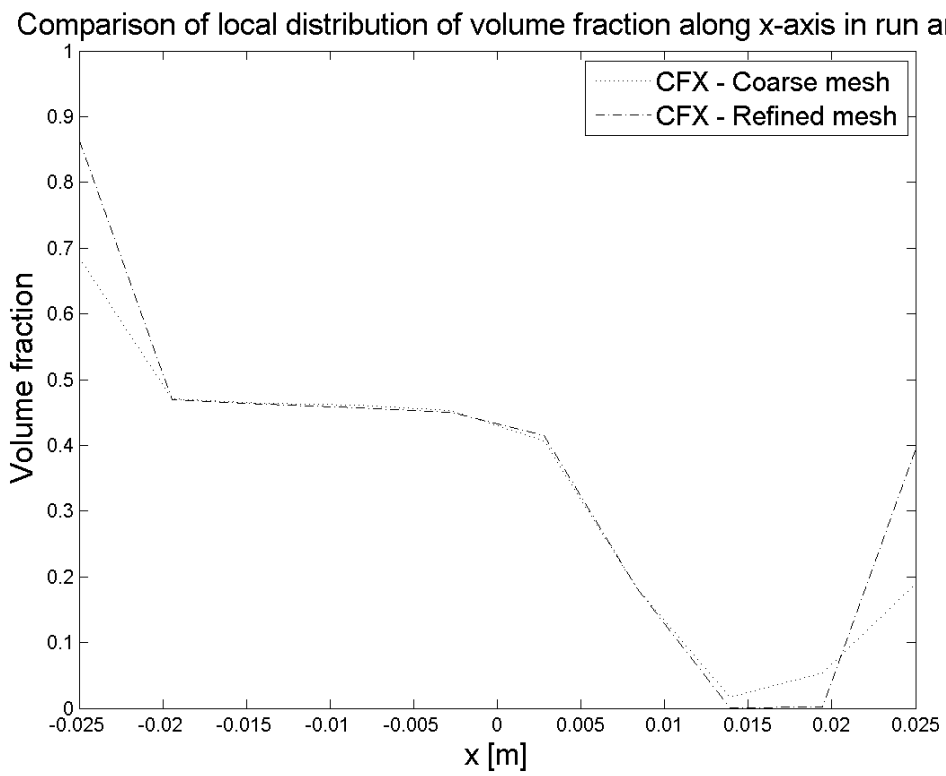

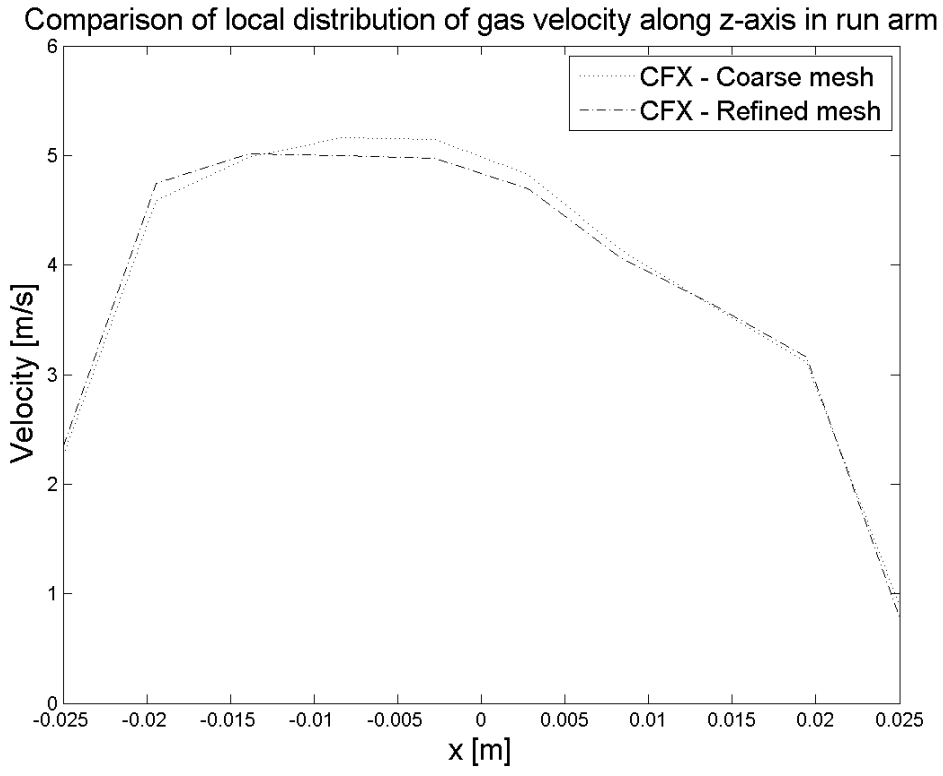

Figure 6.21 Comparison of local distributions along x-axis in run arm for simulation with coarse and refined mesh. Uppermost: Local distribution of volume fraction. Bottommost: Local distribution of gas velocity.

6.5.8 Time formulation

The change in both global parameters and local distribution is very modest for both Fluent and CFX when the time formulation is changed. Figure 6.22 shows contours of volume fraction for the case with a transient time formulation and in Figures 6.23 and 6.24 local volume fraction and gas velocity profiles are compared for the steady state and the transient case. It can be concluded that the results are very similar for the two cases. This indicates that the studied application does not have an extremely transient behaviour and the results from the steady state simulations can be justified.

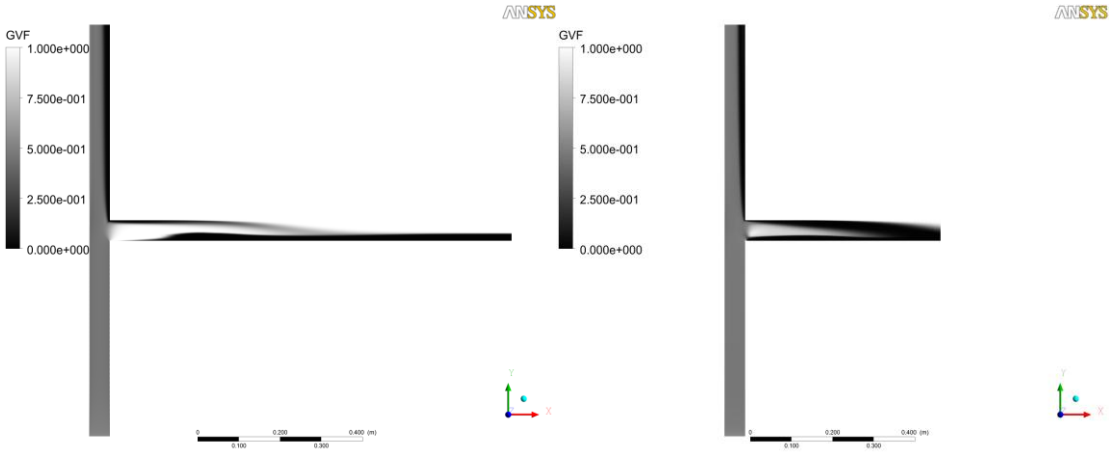

Figure 6.22 Contour plots of volume fraction on mirror plane z = 0. To the left: Fluent Run 10. To the right: CFX Run 10.

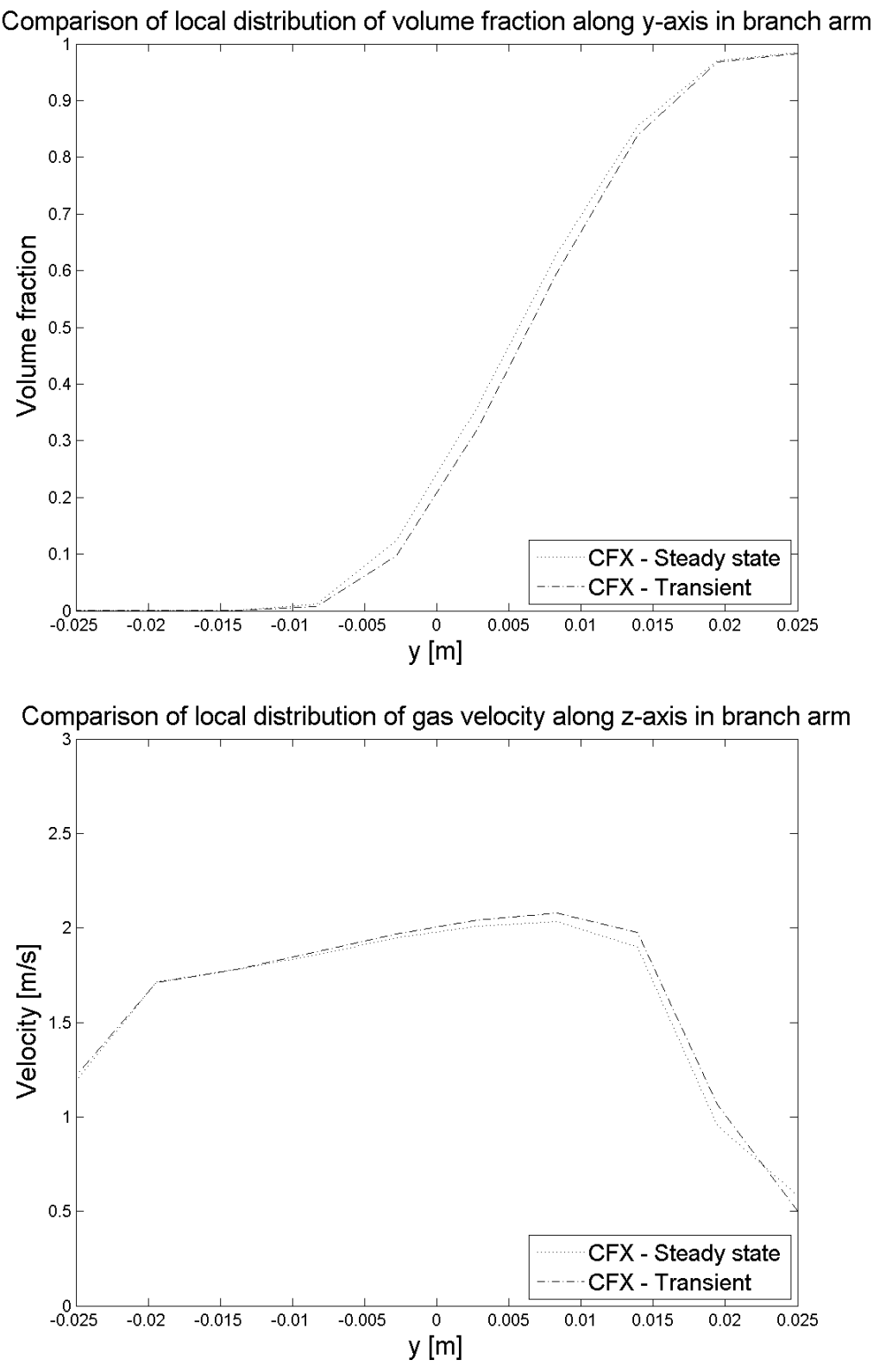

Figure 6.23 Comparison of local distributions along y-axis in branch arm for simulation with a steady state and a transient time formulation. Uppermost: Local distribution of volume fraction. Bottommost: Local distribution of gas velocity.

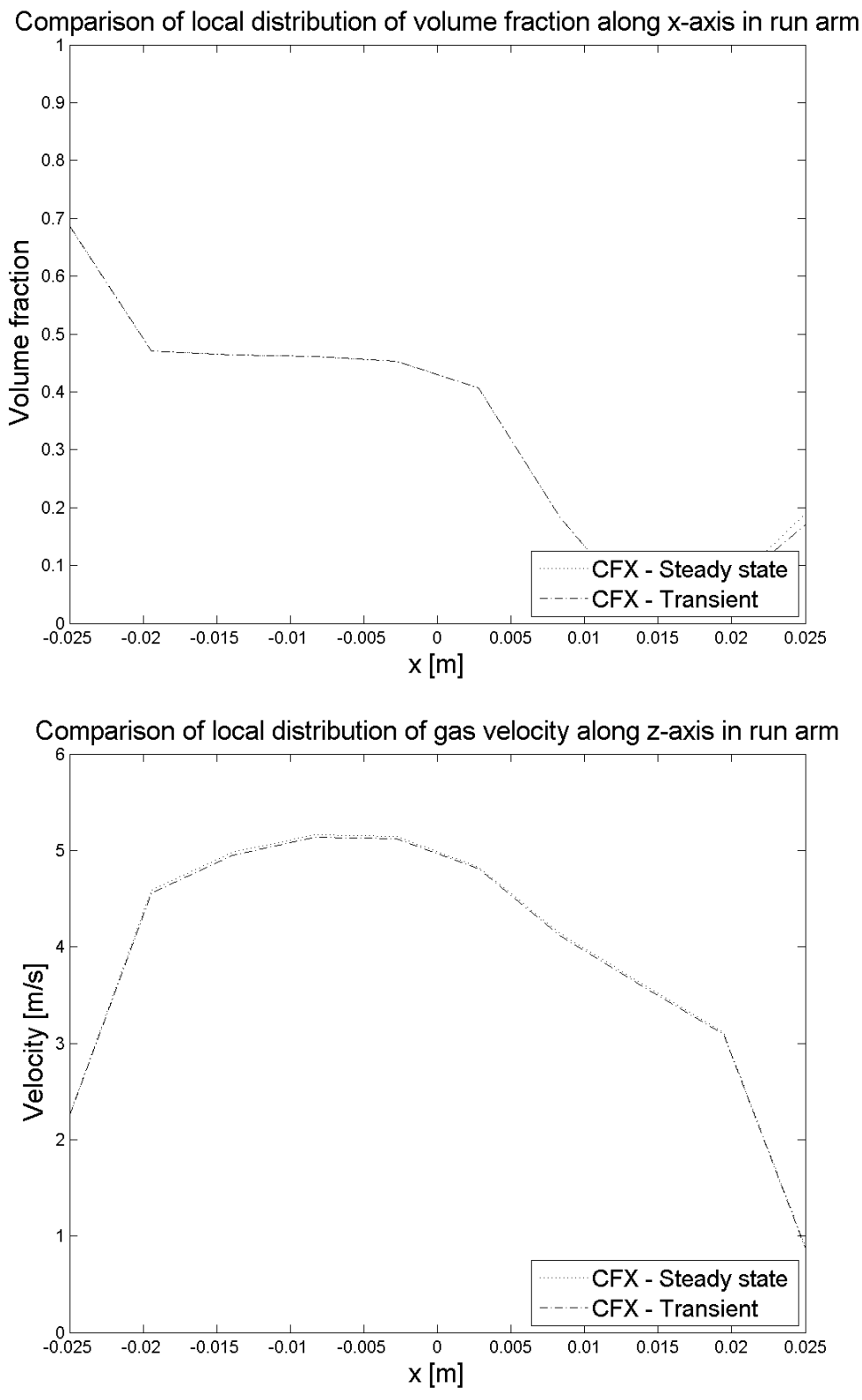

Figure 6.24 Comparison of local distributions along x-axis in run arm for simulation with a steady state and a transient time formulation. Uppermost: Local distribution of volume fraction. Bottommost: Local distribution of gas velocity.

6.6 Investigation of models for polydispersed flow

Generally, agreement with experimental data is improved with polydispersed modelling. However, using two or three constant diameters to represent the polydispersity actually lowered the agreement. Figure 6.25 shows a representative contour plot of volume fraction for cases with polydispersed modelling. It closely resembles the contour plots for the cases where one constant diameter is assumed. One can conclude that the phase redistribution phenomenon does not change when a polydispersed model is included, it is merely the global values and local distributions that changes. The average volume fraction in the branch arm is generally predicted within 10% and for several cases within 5%, see Table 6.1. However, for some cases the volume fraction in the run arm is highly under predicted due to the presence of a large gas free zone along on side of the run arm, this has been discussed in Section 6.3 as well as Section 6.5.6. The largest difference when adding a population balance model can be identified for the velocity field. As previously mentioned, the velocity in the branch arm is under predicted with more than 20% for most cases without polydispersed modelling. With polydispersed modelling, the velocity in the branch arm is predicted within roughly 15% and for several cases within 10%. In the run arm, the average velocity is generally predicted within approximately 10% using a polydispersed model. Using the discrete PBM in Fluent, the average velocity in both run arm and the branch arm is predicted within 6%. These results imply that the effect of polydispersity is strong.

Due to the additional transport equations solved in a polydispersed model, the convergence rate is slower. However, for most simulations the convergence was stable. The main exception was using the IAC model which was numerically unstable and required a good initial guess as well as low of under relaxation factors to converge.

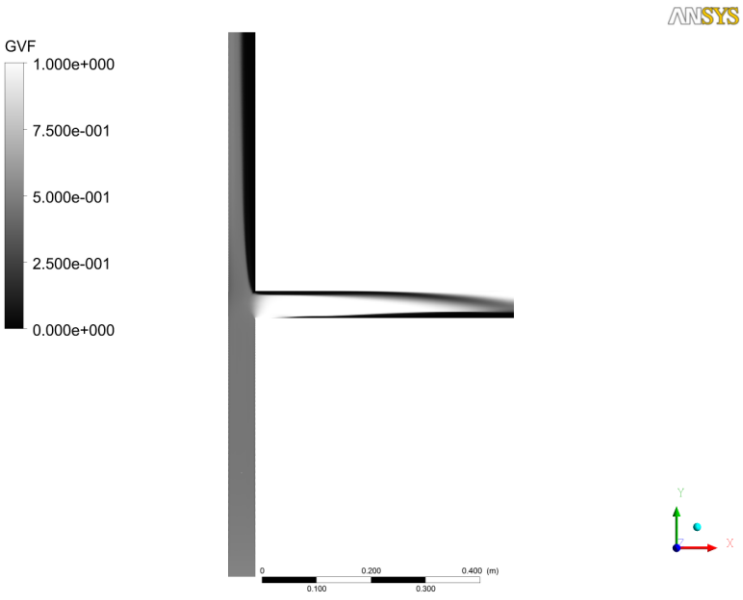

Figure 6.25 Representative contour plot of volume fraction on mirror plane z = 0 for case with polydispersed modelling, CFX Run 15.

6.7 Convergence issues and tips for convergence

As can be seen in Table 6.1 results are not presented for some of the settings. For these settings a converged solution was never obtained. If a simulation did not converge even though it was allowed to run for several thousands of iterations and with manipulation of time step, under relaxation factors, initialisation etcetera, the attempts of finding a converged solution was ended. Further manipulation of initialisation and/or other parameters related to convergence might result in convergence for these cases but due to the limited timeframe during which this project was carried out a restriction in time spent on each individual case had to be made.

For some of the simulations convergence was achieved but with difficulty. This has been discussed in more detail for each setting in Section 6.5. The following strategies were found to be successful for enhancing convergence; lowering under relaxation factors, changing initialisation type, changing time step and starting the simulations without solving the volume fraction equation. Lowering under relaxation factors and changing the initial guess are common ways to enhance convergence, both for single-phase and multi-phase flow simulations (ANSYS Fluent Theory Guide 2011 and ANSYS CFX Theory Guide 2011). Choosing a low time step is also common practice

to improve the convergence behaviour. However, in multiphase flow there is often a great separation of scales, meaning that different flow phenomena can have very different time scales. Therefore, time steps of varying magnitude might be needed to capture the different phenomena. It was found in this study that alternating between a larger and a lower time step could significantly accelerate the convergence rate or even lead to stable convergence for cases that showed highly oscillating residuals when only one low time step was used. This was especially successful in CFX where time stepping is used also for the steady state simulations. For simulations where there was trouble starting up the simulations a good remedy was to start up the simulations without solving the volume fraction equation and letting the velocity and pressure fields develop for some hundreds of iterations before starting to solve the GVF equation.

6.8 Error Sources

Some possible error sources are identified for the numerical simulations. As mentioned in Section 4, it has been shown in several experimental studies that the inlet flow pattern has a great effect on the phase redistribution in the junction. In the CFD simulations, numerical boundary conditions that should represent and correspond to the reality, which in this case is represented by the experiment, are implemented. Due to the complexity of the reality and incomplete information in the article concerning the experiment it is almost impossible to set boundary conditions that exactly correspond to the experiment. If the inlet conditions differ from the experiment it might change the inlet flow pattern which in turn can affect the phase redistribution.

The overall flow split in a T-junction also has a large impact on the phase redistribution. As mentioned in Section 5.2, either a flow split or a pressure condition was set for the outlets depending on the convergence behaviour. For both conditions some adjusting was required to achieve the correct flow split. Hence, the flow split was not exactly 80/20 and the slight difference between the experiment and the simulations can also be responsible for the difference in results.

Due to the limited timeframe of this thesis, no mesh independence study has been made. Therefore, the solution might be dependent on the mesh used and it is possible

that the solution would be in better consistency with the experimental data if another mesh would be used. However, there are conflicting requirements on mesh size regarding multiphase modelling with two-fluid models. As mentioned in Section 6.5.6, the mesh length scale should be significantly larger than the dispersed phase diameter in order to get the averaging in each cell correct. However, to resolve boundary layers and account for the high velocity gradient near the walls a small cell size is needed. This makes the choice of mesh complicated and it could be that with further refinements the solution would become inaccurate.

7 Conclusions

The purpose of this thesis was to compare the multiphase models offered in the ANSYS CFD software Fluent and CFX and investigate the effect of changing simulations parameters through numerical simulations. From the numerical simulations it is evident that the Euler-Euler approach is best suited for the T-junction application. Using an Euler-Euler model the flow redistribution phenomenon was captured in all cases, with the exception of an erroneous prediction of water separation in the run arm. In conclusion, the choice of simulation parameters is not crucial if only the flow phenomenon is of interest, however, for a more detailed analysis the effect of particle diameter and polydispersity was found the be strong. With regards to global parameters the QMOM PBM in Fluent or the MUSIG model with geometric size distribution in CFX were found to be in best agreement with experimental data. However, regarding the local volume fraction and gas velocity profiles the discrete PBM in Fluent was found to be most accurate compared with the experimental data. Generally, it can be concluded that there is a very complex interaction between the phases as well as the simulation parameters when performing numerical multiphase simulations. The importance of specific parameters changes depending on the application studied and it is therefore hard to give any general recommendations on the choice of parameters/settings.

7.1 Future work

To be able to draw firm conclusions and decide which models/settings that work best for the T-junction application a mesh independence should be made for each case. If a mesh independence study is made the possibility that the mesh size is affecting the results is eliminated and a comparison between the settings would be fairer as different models have different requirements on mesh size.

As concluded, multiphase flow simulations involve a large number of parameters and models and due to the limited timeframe many of these parameters have not been investigated in this study. To propose models/settings resulting in better agreement with the experimental data, especially regarding local profiles, a further study could be made on the polydispersed modelling as well as on the effect of adding other forces of interest.

Studies should also be made based on other experiments, especially experiments with other inlet flow patterns than in the experiment this thesis is based on. The VOF/homogeneous models were ruled out quite fast due to the mixed nature of the inlet flow and these models have thus not been as thoroughly examined as the Eulerian/inhomogeneous models. Therefore, studies should be made for cases where a VOF/homogeneous model theoretically should perform better, for example cases with stratified and/or annular inlet conditions.

8 References

ANSYS CFX Solver Theory Guide (2011), 14th release, ANSYS Inc., Canonsburg, Pennsylvania

ANSYS Fluent Theory Guide (2011), 14th release, ANSYS Inc., Canonsburg, Pennsylvania

Arlrachakaran, S.J., Brill, J.P. (1992): State of Art in Multiphase Flow, *Journal of Petroleum Technology*, Vol. 44, No. 5, May 1992, pp. 538-541.

CIA (2013): The World Fact Book, Country Comparison: Refined Petroleum Products –Consumption, https://www.cia.gov/library/publications/the-world-factbook/rankorder/2246rank.html (Collected 2013-04-24)

Crowe, C.T., Schwarzkopf, J.D., Sommerfeld and M., Tsuji, Y. (2012): *Multiphase Flows with Droplet and Particles 2nd edition.* CRC Press, Taylor & Francis Group, Boca Raton, Florida

Davis, M.R. and Fungtamasan, B. (1990): Two-phase Flow Through Pipe Branch Junctions. *International Journal of Multiphase Flow*, Vol. 16, No. 5, January 1990, pp. 799-817.

Elazhary, A.M. (2012): *Two-Phase Flow in a Mini-Size Impacting Tee Junction with a Rectangular Cross-Section,* Ph.D. Thesis. Department of Mechanical and Manufacturing Engineering, University of Manitoba, Winnipeg, Manitoba

Issa, R.I. and Oliveira, P.J. (1993): Numerical Prediction of Phase Separation in Two-Phase Flow through Junctions. *Computers Fluid,* Vol. 23, No. 2, February 1993, pp. 347-372.

Liu, Y. and Li, W.Z. (2011): Numerical Simulation on Two-Phase Bubbly Flow Split in a Branching T-junction, *International Journal of Air-Conditioning and Refrigeration,* Vol. 19, No.4, December 2011, pp. 253-262.

Lundevall, S. (2011): *Integration of a Population Balance Equation into CFD modelling of High Shear Wet Granulation,* M.Sc. Thesis, Department of Chemical and Biological Engineering, Chalmers University of Technology, Göteborg

Mudde, R.F., Groen, J.S. and van den Akker, H.E.A. (1993): Two-Phase Flow Redistribution Phenomena in a Large T-junction, *International Journal of Multiphase Flow*, Vol. 19, No.4, April 1993, pp. 563-573.

Oliveira, P.J. (1992): *Computer Modelling of Multiphase Flow and Applications to T-junctions.* Ph.D. Thesis. Department of Mineral Resources, University of London, London

Saba, N. and Lahey Jr., R.T. (1984): The Analysis of Flow Separation Phenomena in Branching Conduits, *International Journal of Multiphase Flow*, Vol. 10, No. 1, pp.1-20.

Thome, J.R. (2004): *Engineering Data Book III*, Wolverine Tube Inc., Decatur, Alabama, USA

van Wachem, B.G.M. and Almstedt, A.E. (2003): Methods for Multiphase Computational Fluid Dynamics, *Chemical Engineering Journal*, Vol. 96, No. 1, December 2003, pp. 81-98.

Walters, L.C., Soliman, H.M. and Sims, G.E. (1998): Two-Phase Pressure Drop and Phase Distribution at Reduced Tee Junctions, *International Journal of Multiphase Flow*, Vol. 24, No. 5, August 1998, pp. 775-792.